JRC VALIDATED METHODS, REFERENCE METHODS AND MEASUREMENTS REPORT

Recommendation for Creep and Creep-fatigue assessment for P91 Components

MATerials TEsting and Rules
MATTER Deliverable 4.6

Rami Pohja (VTT)
Stefan Holmström (JRC-IET)
Hyeong-Yeon Lee (KAERI)

2016

Report EUR 27781 EN

European Commission
Joint Research Centre
Institute for Energy and Transport

Contact information
Stefan Holmström
Address: Joint Research Centre, Westerduinweg 3, NL-1755 LE Petten, the Netherlands
E-mail: Stefan.holmstrom@ec.europa.eu
Tel.: +31 224 565069

JRC Science Hub
https://ec.europa.eu/jrc

JRC94508

EUR 27781 EN

ISBN 978-92-79-57139-8 (PDF)

ISSN 1831-9424 (online)

doi: 10.2790/49517

Luxembourg: Publications Office of the European Union, 2016

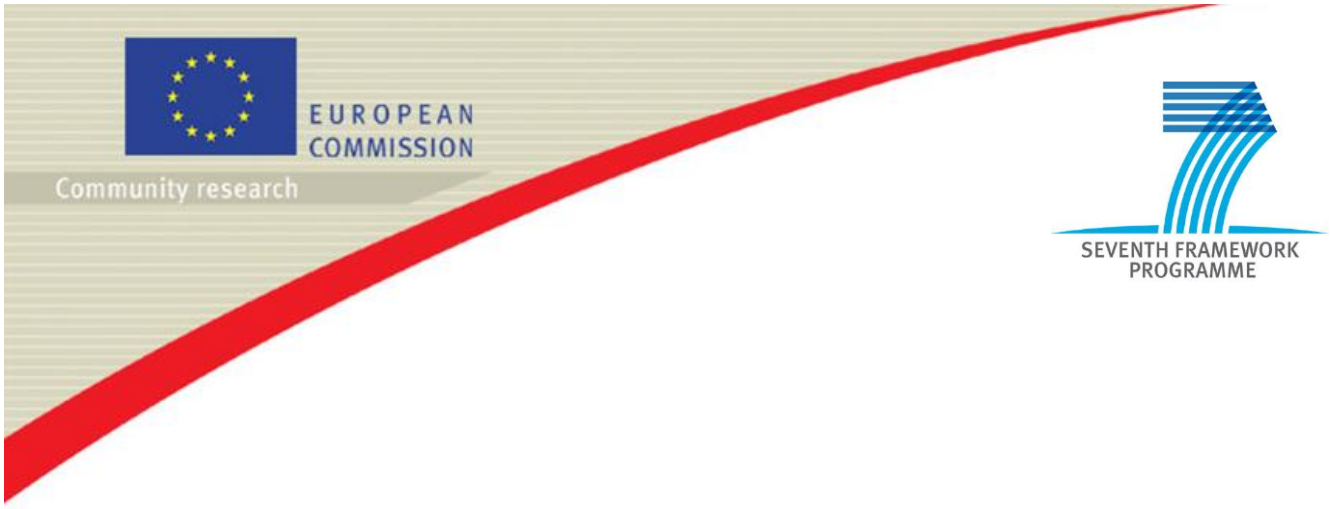

MATTER

MATERIALS TESTING AND RULES – *Grant agreement for collaborative Project*

Co-funded by the European Commission under the
Euratom Research and Training Programme on Nuclear Energy
within the Seventh Framework Programme

Grant Agreement no. 269706
Start date: 01/01/2011 Duration: 48 Months

Recommendation for Creep and Creep-fatigue assessment for P91 Components

Deliverable 4.6

Authors: Rami Pohja, Stefan Holmström, Hyeong-Yeon Lee

Contributors: VTT, JRC, KAERI

Approval:

SEVENTH FRAMEWORK PROGRAMME

MATTER project

EC Scientific Officer: Mykola Džubinský

Document title	Recommendation for Creep and Creep-fatigue assessment for P91 components
Author(s)	Rami Pohja, Stefan Holmström, Hyeong-Yeon Lee
Number of pages	43
Document type	Deliverable
Work Package	WP 4
Document number	D4.6
Date of completion	15/1/2014
Level of Confidentiality	PU ☒ PP ☐ RE ☐ CO ☐
Document Version	1.1

Summary

This report is based on the results and experience gained in assessing both public domain and MATTER data, some previously reported in the MATTER deliverable D4.5: "Creep-fatigue interaction rules for P91" and some assessed here. A number of methods, including interaction diagram based methods and simplified methods, have been compared for predicting the creep-fatigue life of P91 steel. The effect of cyclic softening on creep properties have been considered in the evaluations presented in this report. The purpose of this report is to give recommendations for creep and creep-fatigue assessment for components made of X10CrMoVNb9-1 (P91) steel. Based on the conclusions of the assessments the following recommendations are given:

1. The creep properties of P91 steel suffer from cyclic loading and it is recommended that the current RCC-MRx creep strain equations should be modified or replaced by a model that can implement time factors or stress reduction factors to correct for softening. Suitable models have been identified. The softening of P91 potentially causes unconservativeness in significant creep conditions where accumulated strain is a limiting design factor.
2. The interaction diagram models currently applied in design codes are complicated to apply and include several complex modelling challenges. It has been recommended that alternative modelling concepts, such as using simplified models should be considered for use in design codes. The simplified models optimized for P91 have been shown to give good and robust predictions on cycles to failure.
3. Currently available P91 data mainly consists of large strain range and short hold period data, where creep is mainly causing additional strain. Data with verified creep cavitation damage is limited or totally lacking. It is recommended that more data is generated at low strain ranges and long hold times to improve long term extrapolation robustness. Tensile property data for softened material is also needed to determine the stress range where power-law breakdown behaviour in creep can be expected and to improve the understanding of the long term microstructural evolution in cyclic service.

Revisions

Rev.	Date	Short description	Main author	(WP Leader)	DP Leader

Distribution list

Name	Organisation	Comments
Dzubinsky, Mykola	EC	Scientific Officer
Utili, Marco	ENEA	Scientific Responsible Domain Leader -4
Agostini, Pietro	ENEA	Project Coordinator
Colombarini, Mara	ENEA	Assistant for the Project Organization
Gavrilov, Serguei	SCK CEN	Domain Leader – 1
Giacomo, Aiello	CEA	Domain Leader – 2
Angelika, Bohnstedt	KIT	Domain Leader – 3
Malerba, Lorenzo	SCK•CEN	EERA JPNM coordinator
Gelineau, Odile	AREVA	Workpackage Leader – 1
Chen, Jia-Chao	PSI	Workpackage Leader – 2
Lambrinou, Konstantza	SCK CEN	Workpackage Leader – 3
Ancelet, Olivier	CEA	Workpackage Leader – 4
Aktaa, Jarir	KIT	Workpackage Leader – 5
Barbieri, Giuseppe	ENEA	Workpackage Leader – 6
Davide Bernardi	ENEA	Workpackage Leader – 7
Nilsson, Karl-Fredrik	JRC	Workpackage Leader – 9
Serrano, Marta	CIEMAT	Workpackage Leader – 10
Maday, Francoise	ENEA	Workpackage Leader – 11
Warwick, Payten	ANSTO	
Sophie, Dubiez-Legoff	AREVA	
Marie, Stéphan	CEA	
Lebarbé, Thierry	CEA	
Blat, Martine	EDF	
Dean, David	EDF-UK	
Pillot, Sylvain	Industeel	
Lee, Hyeong-Yeon	KAERI	
Hoffelner, Wolfgang	retired	
Pohja, Rami	VTT	
Auerkari, Pertti	VTT	
Dundulis, Gintas	Lithuanian Energy Institute	

Table of Contents

1 Introduction

Creep-fatigue (CF) damage can be evaluated using the rules and guidelines provided in the existing design codes, such as ASME III NH, RCC-MRx and BS-R5. Commonly the rules are based on the creep-fatigue interaction diagram and the methods differ in the way how the creep and fatigue damage fractions are calculated. For RCC-MRx, it should be noted that the Tome 6 of the RCC-MRx 2012 edition states that the code rules for interaction between fatigue and creep are not satisfactory defined from the point of view of safe design using X10CrMoVNb9-1 steel. This originates from test results which have recently become available, which indicate that the behaviour of such steels with cyclic strain softening makes it a non-conservative option to apply the alternative rule for progressive deformation when determining the effective primary stress according to code sections RB 3261.1111 to 1117 and RB 3262.1111 to 1117. It is stated that there is a need to redefine a method and/or a criterion for an alternative rule justifying the absence of progressive deformation and, in general terms, extend the knowledge of cyclic behaviour of such steels at elevated temperatures. Whilst awaiting the results of research and analysis on this subject so as to prevent the use of progressive deformation rules for this steel, it has been decided to incorporate the corresponding material properties and assessment rules, including cyclic curves, fatigue curves, creep strain rules and creep-fatigue interaction diagram, earlier stated in appendix: A3.18AS – cyclic behaviour and creep, in the probationary phase rules [1].

A number of methods were compared for the predicting the creep-fatigue life of P91 steel in the report “Creep-fatigue interaction rules for P91” [2] using public domain data and data produced in projects prior to the MATTER project. Some further assessments with some newly developed and classical methods were also assessed in the ASTM paper [3] by MATTER consortium authors. It is common practice in all the mentioned design rules to assess the creep-fatigue interaction with an interaction diagram. The interaction diagram approach is based on separate creep and fatigue assessments where the interaction is taken by the interaction diagram. The diagram does not have any physical basis and the scatter in the predictions is quite large.

It has been shown that the time fraction approach for interaction (using RCC-MRx locus point (0.3,0.3), which is now in the probationary phase rules of the code) performs satisfactorily and that the classical ductility exhaustion method (DE) predicts extensive creep damage. The modified ductility based versions (SMDE and EMDE) performed better than the classical approach. A strain rate modified (SRM) model with time dependent damage accumulation also shows promise for use in creep-fatigue interaction diagrams.

Application of the rules of ASME III NH and RCC-MRx rules to P91 components showed that the ASME III NH rules are more conservative than those of RCC-MRx. Creep evaluation procedure of ASME III NH requires in comparison to RCC-MRx a more conservative interaction diagram with respect to allowable creep damage in the presence of fatigue for considering the effects of cyclic softening shown by this type of steel [4], [5].

It has also been shown that good and robust predictions of the CF number of cycles to failure for Grade 91 steel can be accomplished by simplified methods [3], [6], [7], [8]. These models utilize much fewer fitting parameters than the methods included currently in design codes. If considering

the clear difference in total amount of fitting constants for simplified models and those of the different interaction models it seems clear that the simplified methods have an advantage when selecting models for implementation in design codes. In the case of the simplified methods they currently predict only constant-amplitude strain data. However, these methods can be extended to take into account the specifics of varying cycle types.

The design and assessment tools for creep-fatigue assessment do not have to rely on the same models. Design rules have to give concise simple rules to guide the selection of component dimensions and materials and they need to be conservative but not overly conservative. The very large scatter in predictions from the design rules in combination with safety margins may lead to very conservative designs. It should also be kept in mind that almost all laboratory creep-fatigue data are for relatively short hold times with a large fatigue damage factor and may therefore not be good measures for the predictability of creep-fatigue models when creep dominates. The creep fatigue tests with the relatively short hold times in stress control do produce extensively larger creep strains than corresponding relaxation tests but the "creep damage" attained is mainly strain, not creep cavitation damage in the grain boundaries that causes intergranular fracture and reduced material ductility. The extrapolation to the more "long term" type of creep damage is thus questionable.

An important feature of any model and methodology to be incorporated in design codes is that the rules and calculations need to be simple and conservative, though not overly conservative. Especially the relaxation behaviour and creep damage assessment methods and the safety factors related to them have very strong impact on the estimated total creep-fatigue damage. Reasonable safety margins must be included and verified against reliable data for safe design and operation of generation IV solutions.

2 Testing activities to support assessment and modelling

A considerable amount of tests to investigate the creep-fatigue properties of P91 steel was conducted by project partners during the MATTER project. The creep-fatigue test types included:

1) Standard low cycle fatigue tests in strain control (LCF).
2) Creep-fatigue tests with hold period, for which the cycling was conducted in strain control and the hold time remained in strain control (to introduce stress relaxation during the hold period).
3) Creep-fatigue tests with hold times, for which the cycling was conducted in strain control and the hold period was conducted in stress control (to introduce "forward" creep during the hold period).

Furthermore, a set of conventional creep tests and fully (engineering) stress controlled LCF tests were conducted to support the investigation of creep-fatigue properties of P91 steel. For stress controlled LCF tests, the interpretation of these tests is more difficult to conduct due to additional complexity introduced by ratcheting. The ratcheting leads to rapid strain accumulation at higher stresses and tests are usually terminated due to reaching the testing machine extensometer strain

limitations. A more detailed description of testing activities performed in the MATTER project is given in the MATTER Deliverable report D7.1 [9].

3 Current assessment methods

The models and methodologies included currently in design codes utilize the creep-fatigue interaction diagram and the methods differ in the way how the creep and fatigue damage fractions are calculated [1], [4], [10]. In ASME-NH, DDS and RCC-MRx the calculation procedure of creep damage utilizes the time-fraction approach. The RCC-MRx and DDS procedure are similar, whereas ASME-NH is considerably different in that it uses isochronous stress-strain curves. The R5 procedure is based on a ductility-exhaustion methodology and is currently the only code following this technique. These procedures use the results of creep tests to determine the creep damage-accumulation models, which are subsequently applied to predict damage in creep-fatigue cycling and in particular strain-controlled dwells that arise during steady operation within a thermal cycle. For time-fraction approaches, the rupture strength of the material is used to calculate creep damage, while in the ductility-exhaustion approach the creep ductility is used to calculate creep damage.

The interaction diagram for P91 as defined by RCC-MRx probationary phase rules and ASME-NH is presented in Figure 1 with the creep damage defined as t/t_r and the fatigue fraction as N_f/N_{f0}. In the different design rules the N_{f0} (LCF cycles to failure from testing) is replaced by an allowable number of cycles for design. It is as earlier mentioned important to keep in mind that the clearly different interaction locus points are not describing a different view of material endurance between the codes but is a product of entirely different calculation methodologies for creep damage accumulation. Additionally, the RCC-MRx locus point (0.3,0.3) should be taken as a probationary phase rule.

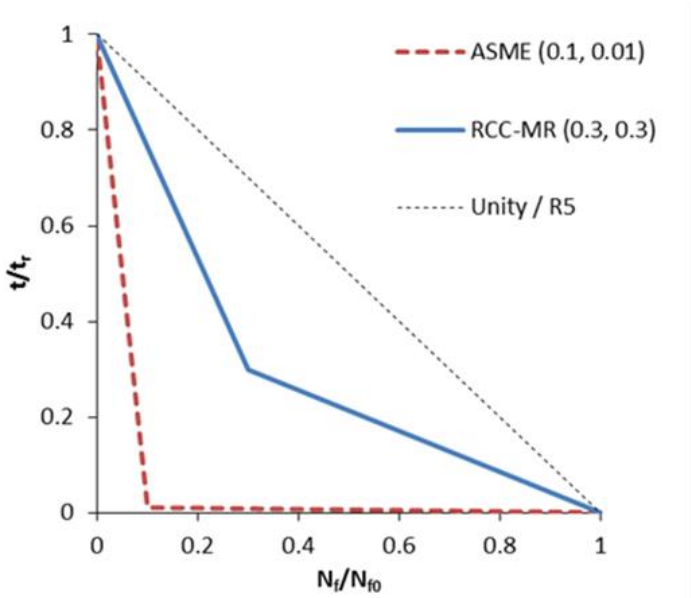

Figure 1. The creep-fatigue Interaction diagram for P91 as defined by nuclear codes.

3.1 Fatigue models and allowable cycles

In nuclear codes fatigue curves indicating the allowable number of cycles as functions of strain ranges at relevant temperatures are provided for fatigue assessment. Fatigue design curves given in the ASME Code Section III are derived from reference mean curves, which are based on strain controlled low cycle fatigue tests. Arbitrary design margins, 20 against life and 2 against strain, were considered appropriate for ensuring transferability of the data to plant components, as by ASME (1972) [11]. Similar curves are included also in the European design codes, such as RCC-MRx.

Outside the codes, a common practise to predict the number of fatigue cycles to failure is to use empirically based simplified fatigue models, such as Langer curve [12] and Manson-Coffin [13], for steels for which a large number of fatigue data is available for model fitting. The Langer curve is defined in Equation (1):

$$\Delta\varepsilon_{fat} = \Delta\varepsilon_0 + a \cdot N_f^b \tag{1}$$

Where $\Delta\varepsilon_{fat}$ is the applied fatigue strain range, $\Delta\varepsilon_0$ is the maximum strain range for which the fatigue lifetime remains infinite as assumed in this model, N_f is number of cycles to failure, a and b are fitting parameters.

The LCF Manson-Coffin model for cycles to failure N_{f0} is defined as:

$$N_{f0} = \left[\frac{(\Delta\varepsilon - C_1)}{C_2}\right]^{1/C_3} \tag{2}$$

Where C_i are the fitting parameters and $\Delta\varepsilon$ is the total strain range.

The creep-fatigue tests performed for P91 steel in strain control with hold time in strain control were the main test type of the MATTER project. The tests were concentrated on the temperatures of 550°C and 600°C. A detailed description of the LCF and CF tests performed in MATTER project is provided in [9]. The MATTER LCF tests were situated in the strain-cycles to failure plots close to the mean line and always within the scatter range of the JAEA test data [14] as can be seen in Figure 2. The allowable number of cycles as a function of strain range as defined in the probationary phase rules in RCC-MRx code is also shown in Figure 2. The Manson-Coffin parameters for the JAEA and MATTER data are given in Table 1 for 550 and 600°C for the MATTER data and 550 and 625°C for JAEA and EPRI [15] data. Note that the amount of data was not sufficient in the low strain range end for temperatures 600 and 625°C to find reasonable values for the fatigue limit, thus a value of 0.24 was set for the c_1 parameters.

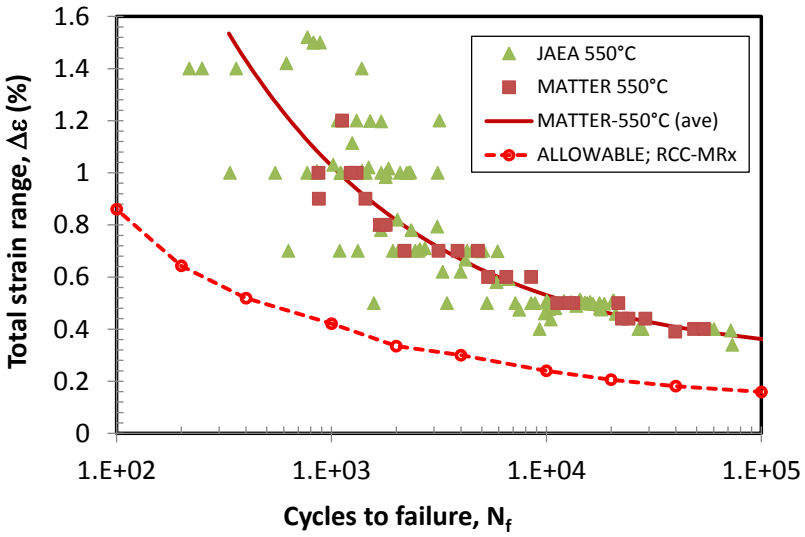

Figure 2. The MATTER LCF test data (550°C) and Manson-Coffin model in comparison to the JAEA test data [14].

Table 1. Parameters for the Manson-Coffin model. Parameters optimized on JAEA, MATTER and EPRI (625°C) data.

Temp. (°C)	c_1	c_2	c_3
550 (MATTER)	0.27472	19.17968	-0.46885
550 (JAEA)	0.23976	33.39224	-0.52268
600 (MATTER)	0.24	148.6077	-0.72138
625 EPRI	0.24	142.2743	-0.76605

The CF tests performed in MATTER project are presented in the strain-cycles to failure plots in Figure 3. The hold time was applied either in tension, compression or both. The tests with hold times in tension or both tension and compression gave for this data set the shortest cyclic lives,

partly contradicting the findings of [16] stating that the oxidation growth on the specimen in compression hold decrease the crack initiation times the most. It is to be noted that the MATTER tests have rather short hold times (600-1820 s) and short cyclic lives, in many cases less than 2000 cycles. The hold times were perhaps not long enough to produce oxide scales of the magnitude causing premature cracking.

Even with hold periods, all the data points resided above the allowable limit defined in the probationary phase rules of RCC-MRx code. However, a majority of assessed data is in the parameter range, where the total strain range is relatively large (> 0.4%). In real plant conditions the total strain ranges are expected to be lower and the hold periods significantly longer. Thus, it is rather difficult to evaluate the safety margins of the allowable fatigue limits of nuclear codes within relevant parameter range using test results with large strain ranges and short hold periods.

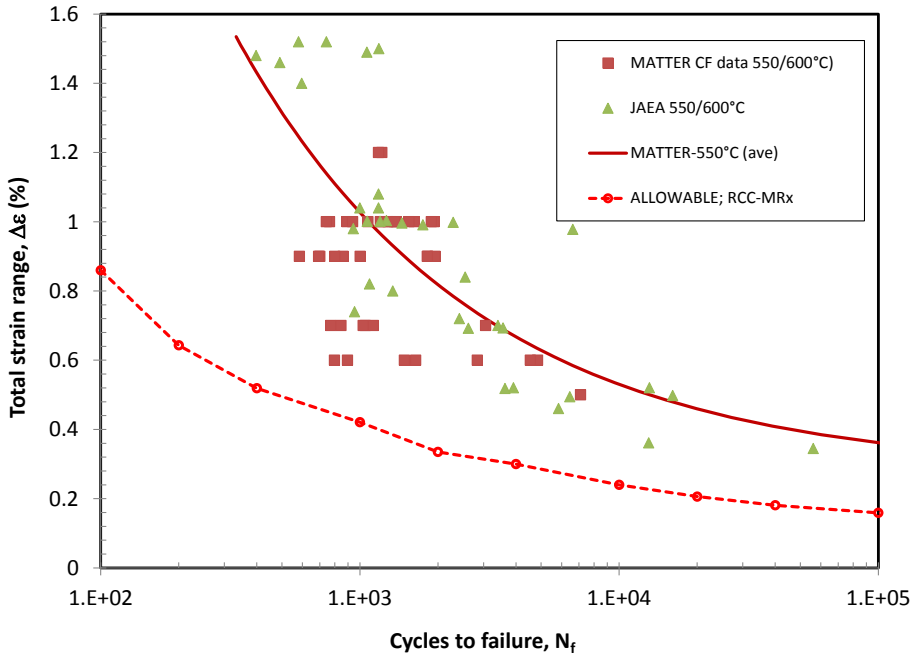

Figure 3. The MATTER CF test data (550 and 600°C) with hold times between 0.1 and 1 h in comparison to JAEA test data [14] (hold times between 0.1 and 1 h) at the same test temperatures. Note: The lowest number of cycles to failure were measured with ridged specimen with hold time in tension ($\Delta\varepsilon$=0.6%, t_h~1820s) or in both tension and compression ($\Delta\varepsilon$=0.7% and 0.9%, t_h~600s).

Figure 4 and Figure 5 show design curves of ASME, RCC-MRx and DDS and fatigue data at 550 and 600°C, which includes test results also from small strain range area (0.2-0.4%) [14]. The data set includes results from different laboratories, material heats and testing conditions. A set of test specimens had been thermally aged at 550°C for up to 75000h, which did not seem to have significant effect on fatigue life. However, fatigue life showed clear strain rate dependency. As strain rate became slower, fatigue life became shorter. It should be noted, that EPRI data at 550°C showed shorter fatigue lives, some points even close to the ASME design curve. In general, when average curves of test results were compared to the nuclear code design curves, the safety margin appeared to be 1 – 2 orders of magnitude (T = 550-600°C, Δε = 0.2-1.0%).

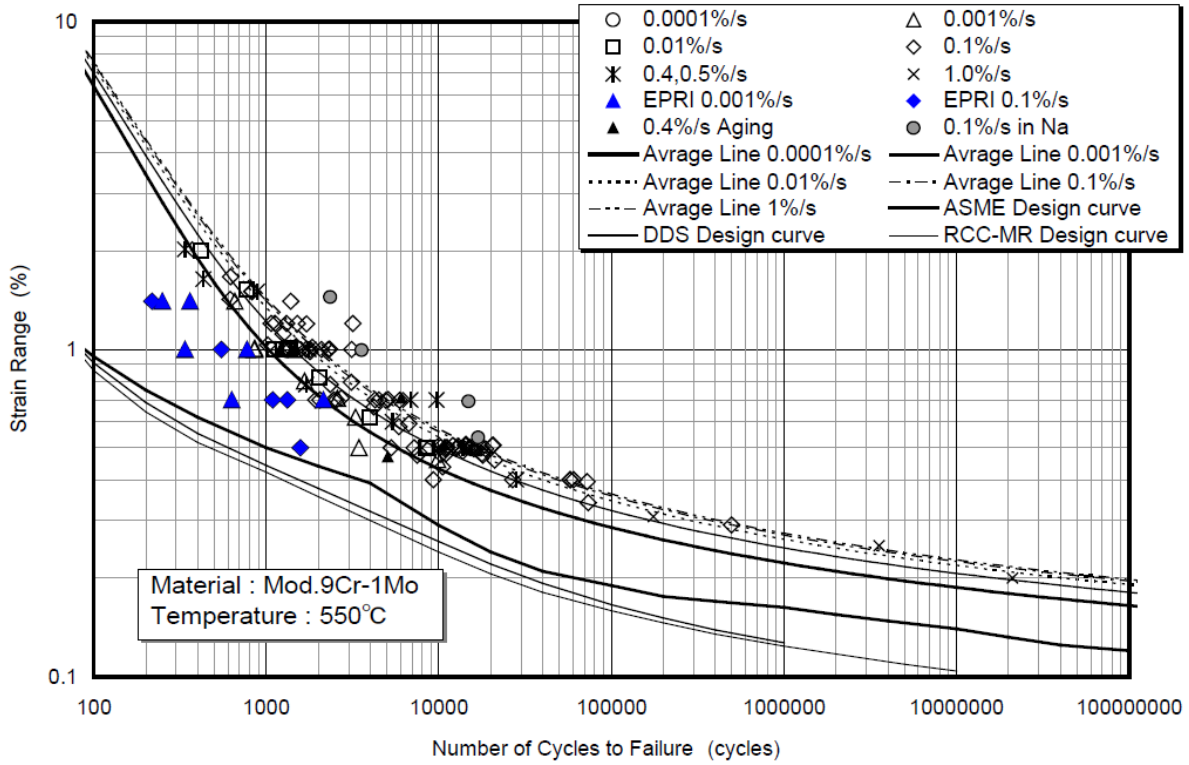

Figure 4. Fatigue life: Design curves, average curves and experimental values at 550°C [14].

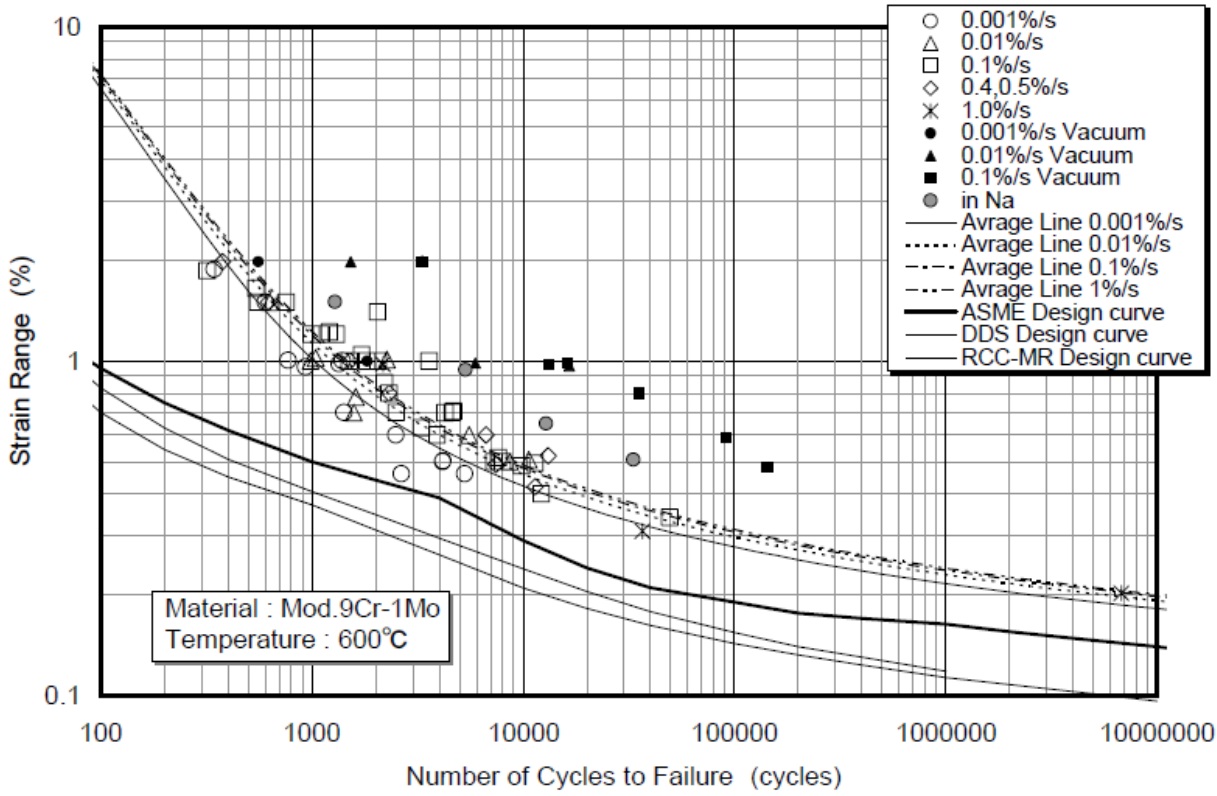

Figure 5. Fatigue life: Design curves, average curves and experimental values at 600°C [14].

3.1.1 Strain range amplification due to creep

In MATTER project it was found that for the P91, as also shown in earlier results for this steel [17], the relaxation or forward creep strain (with relatively short hold periods) is in fact mainly enlarging the hysteresis loops during the CF hold time. In RCC-MRx, in the guide for prevention of fast fracture (A16.727.1) [18] for cycles to creep-fatigue crack initiation the amplification of strain range due to creep is calculated as:

$$\Delta\varepsilon_i = \Delta\varepsilon_e + \Delta\varepsilon_p + \Delta\varepsilon_c \tag{3}$$

For strain control hold time (in tension) the creep strain amplification is calculated as:

$$\Delta\varepsilon_c = \frac{\sigma_{pN_{f/2}} - \sigma_{rN_{f/2}}}{E} \tag{4}$$

Where E is the young's modulus at the specific test temperature.

For stress controlled hold time (in tension) the creep amplification is:

$$\Delta\varepsilon_c = \varepsilon_{totN_{f/2}} - 0.5 \cdot \Delta\varepsilon \tag{5}$$

When presenting the CF data in $\Delta\varepsilon_i$ instead of $\Delta\varepsilon$ the data points will move vertically upwards in the strain-cycles to failure plots. In many cases the result will move closer to the LCF data average curves and in some, especially at high strain ranges, above the LCF curve. In [17] the same approach was used, with the elastic strain range removed, and it was shown that for P91 the shorter lives measured in CF tests were in fact only due to the increase of viscoplastic strain and the damage mechanism remained similar to LCF tests.

In Figure 6 the strain controlled CF tests done by JRC are presented in creep amplified strain range $\Delta\varepsilon_i$ calculated from the relaxation at $N_f/2$ cycles. It is to be taken into account that both the "relaxed strain" and the creep strain in stress controlled tests vary from cycle to cycle and $N_f/2$ has been chosen to represent the whole test.

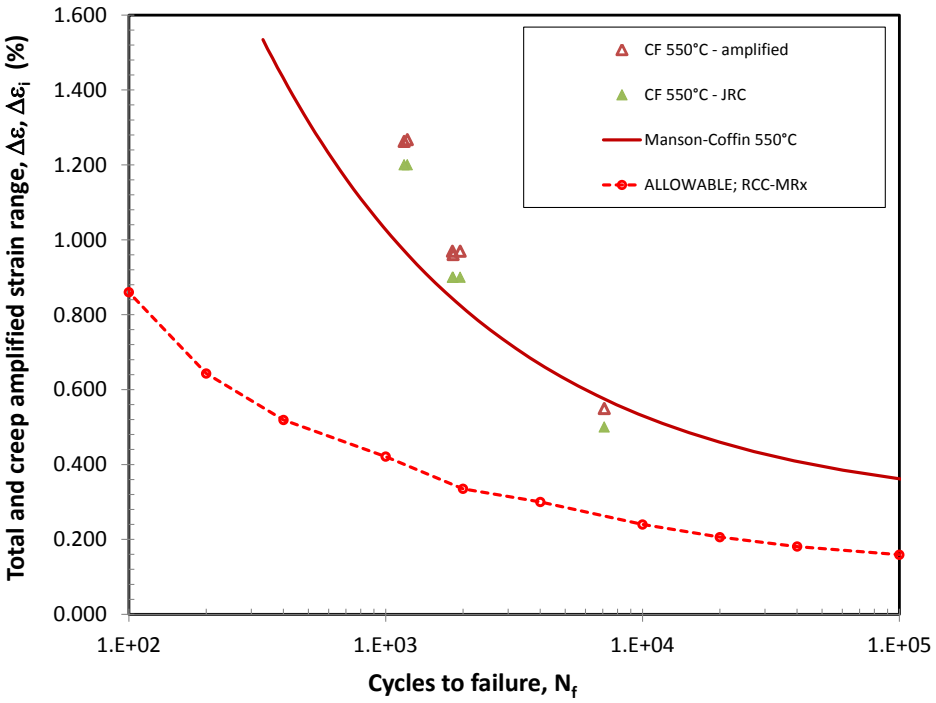

Figure 6. The JRC CF test data (550 and 600°C) with hold times between 0.1 and 0.34 h in presented in total ($\Delta\varepsilon$) and creep amplified ($\Delta\varepsilon_i$) strain range.

For the stress controlled hold times the impact of the creep amplification is larger. The CF tests from MATTER and [16] are presented in Figure 7 with and without creep strain correction. Also in [16] it was concluded that the main damage present in the test is due to viscoplastic deformation to a much larger extent than to creep cavitation from diffusion processes.

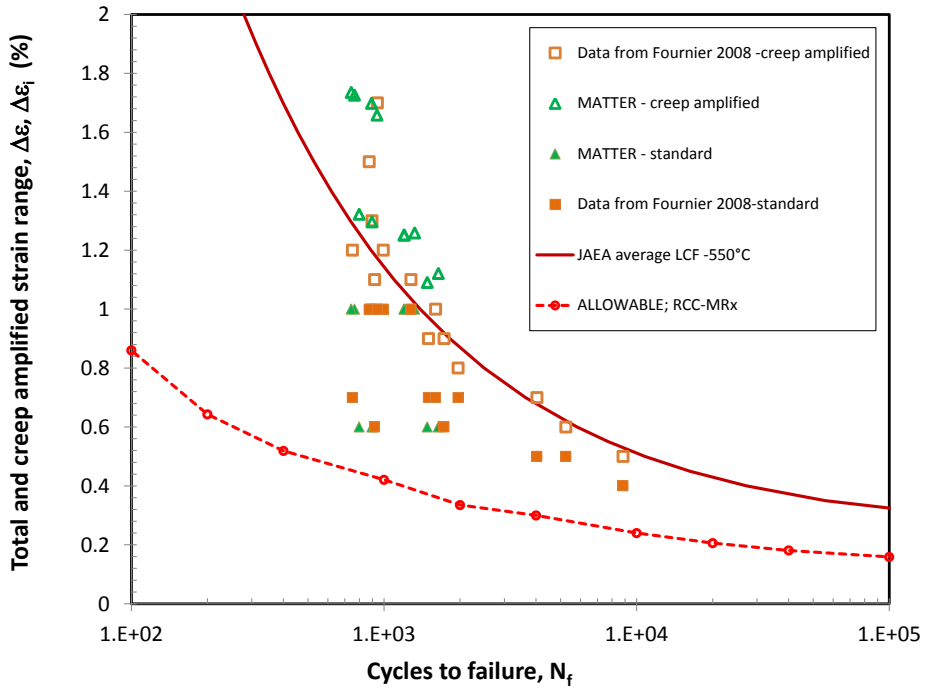

Figure 7. The JRC CF test data (550 and 600°C) with hold times between 0.1 and 0.34 h and test data from [16] presented in total ($\Delta\varepsilon$) and creep amplified ($\Delta\varepsilon_i$) strain range.

From the creep amplified presentation of relaxation and forward creep hold periods in CF tests it could be concluded that the actual creep (cavitation) damage of the tests are negligible since the amplified data plots are well represented by the LCF model. However, for using this method it is necessary to have either the actual hysteresis data or models that can describe the complex relaxation process in the softening material. The main challenge of the method for general CF interaction prediction is the likely limitations of applicability due to extrapolation into the range where creep cavitation and intergranular cracking is to be expected. These factors are basically also a challenge for using this simple method in design rules. It could be argued that there is in fact not enough data in the relevant long term creep-damage range to model and predict the creep dominated interaction with fatigue.

3.2 Creep assessment and modelling

3.2.1 Creep strain modelling

Creep strain sets design limits for many components in power engineering, such as for blading, bolts and casings of steam and gas turbines. In addition, creep strain is also an important quantity to be followed for the fit-for-service inspections and follow ups of critical power plant components. The typical recommended limits range up to 1-2% of strain. However, measuring local strain and predicting it in critical locations is not a simple task. The on-line monitoring equipment have today evolved to perform well, for instance, in the measurement of thick-walled high temperature components, but they are expensive and are of course not standard equipment in new installations. Also, the challenge would be to know where the most critical locations are. From the FEA point of view the main contributor that creep modelling is not done very frequently

is the short supply of relevant creep data and/or parameters for existing (implemented) creep routines.

In the probationary phase rules of RCC-MRx [1] the creep strain in the primary creep regime in the temperature range of 375-600°C is calculated with the Equation (6):

$$\varepsilon_{fp} = C_1 t^{C_2} \sigma^{n_1} \tag{6}$$

In this Equation, ε (%) designates the creep strain attained under stress σ (MPa) after time t (h) at temperature T (°C). The creep strain rate at the primary creep regime, assuming a strain hardening behaviour, is calculated by the Equation (7):

$$\dot{\varepsilon}_f = K \varepsilon^x \sigma^y \tag{7}$$

The coefficients C_1, C_2, n_1, K, x and y are functions of temperature and they are provided in the RCC-MRx code and shown in Table 2. The end of primary creep (t_{fp}) is given in Equation (8):

$$t_{fp} = C_3 \sigma^{n_3} \tag{8}$$

The coefficients C_3 and n_3 are functions of temperature and they are provided in the RCC-MRx code and shown in Table 2. In the secondary creep regime, where the temperature is 375°C or higher and the creep time is greater than t_{fp}, the creep strain is calculated with the Equation (9).

$$\varepsilon_{ffp} = \varepsilon_{fp} + C \sigma^n (t - t_{fp}) \tag{9}$$

The creep strain rate at the secondary creep regime is calculated by the Equation (10):

$$\dot{\varepsilon}_s = C \sigma^n \tag{10}$$

The coefficients C and n are functions of temperature and they are provided in the RCC-MRx code and shown in Table 2.

Table 2. The coefficients for calculating the creep strain according to the rules of RCC-MRx code [1].

T (°C)	C_1	C_2	N_1	n	C	K	x	y	N_3	C_3
375	8,11E-18	0,2734	6,0134	11,1716	1,06E-35	8,37E-64	-2,6568	21,9956	-7,099	6,86E+23
400	9,61E-17	0,2833	5,6934	10,6611	1,99E-33	8,14E-58	-2,5301	20,0979	-6,9313	3,27E+22
450	1,30E-14	0,3029	5,0577	9,7461	2,35E-29	4,41E-47	-2,3011	16,6963	-6,7259	2,38E+21
475	1,4E-13	0,3127	4,7421	9,3345	1,59E-27	2,97E-42	-2,1982	15,166	-6,6816	3,9E+19
500	1,685E-12	0,3224	4,4279	8,9495	8,25E-26	9,75E-38	-2,1019	13,7347	-6,6729	8,27E+18
525	1,884E-11	0,3321	4,1152	8,5886	3,31E-24	1,67E-33	-2,0116	12,3931	-6,6973	2,37E+18
550	2,083E-10	0,3417	3,8038	8,2497	1,07E-22	1,58E-29	-1,9268	11,133	-6,7532	9,04E+17
575	2,277E-09	0,3513	3,4939	7,9307	2,82E-21	8,72E-26	-1,847	9,9471	-6,8389	4,49E+17
600	2,462E-08	0,3608	3,1854	7,63	6,16E-20	2,94E-22	-1,7717	8,8293	-6,9531	2,87E+17

The probationary phase rules of RCC-MRx define the limits of allowable stress (MPa) as a function of the temperature and time t as shown in Table 3.

Table 3. Allowable stress as a function of temperature in the RCC-MRx probationary phase rules [1].

θ (°C)	1 h	10 h	30 h	100 h	300 h	1000 h	3000 h	10^4 h	3.10^4 h	10^5 h	3.10^5 h
425	296	288	284	280	276	268	249	229	212	195	180
450	286	279	275	272	256	236	218	200	184	167	153
475	265	252	246	240	224	207	190	173	158	143	129
500	244	226	218	210	195	179	165	149	134	120	107
525	229	213	198	181	167	158	138	124	112	100	88
550	219	186	171	155	141	127	114	101	89	78	68
575	192	160	145	130	117	103	92	79	69	58	49
600	167	136	122	108	95	82	71	60	51	42	34
625	143	112	97	84	73	63	54	44	36	29	
650	112	80	69	58	49	41	35	29	24		

Creep tests performed for P91 [19] steel were evaluated using the creep rules provided in the RCC-MRx code. The creep strain was calculated for each test according to the RCC-MRx procedure described above and the results were compared against the measured creep strain values as shown in Figure 8 and Figure 9. It should be noted that in some cases the stress levels exceed the allowable stress limits shown in Table 3. However, in the RCC-MRx code the stress relaxation during a hold period is calculated utilizing the creep strain rules. Thus, to be able to perform creep-fatigue interaction assessment including stress relaxation evaluation for CF tests in MATTER parameter range, the creep strain rules have to be applied and stress levels shown in Figure 8 and Figure 9 are relevant for that type of assessment.

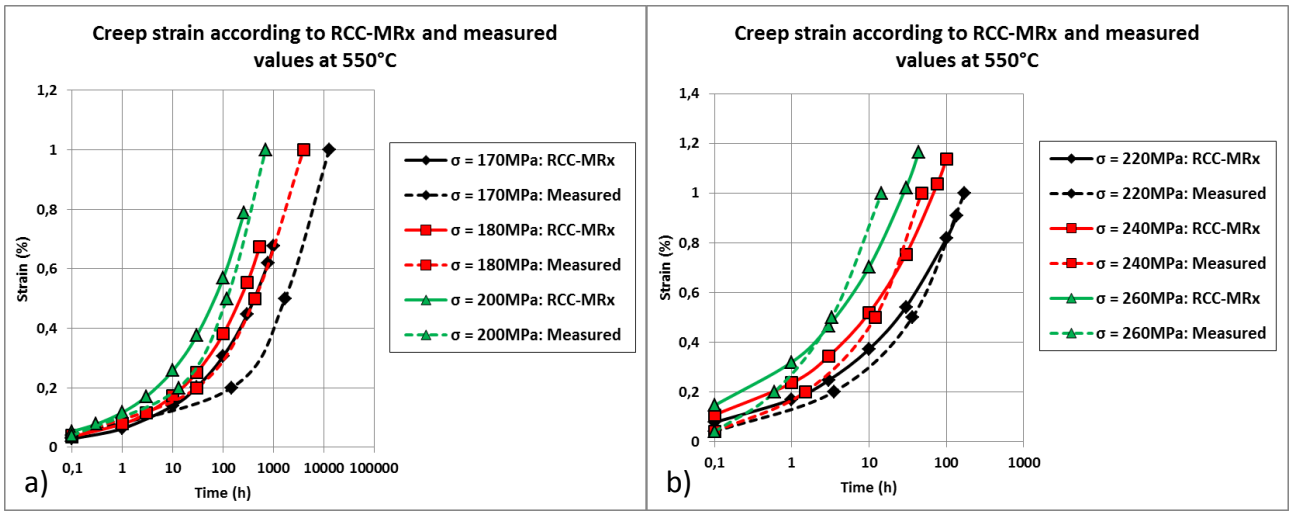

Figure 8. Creep test results for P91 steel at 550°C and creep strain according to RCC-MRx probationary phase rules for a) 170-200MPa and b) 220-260MPa.

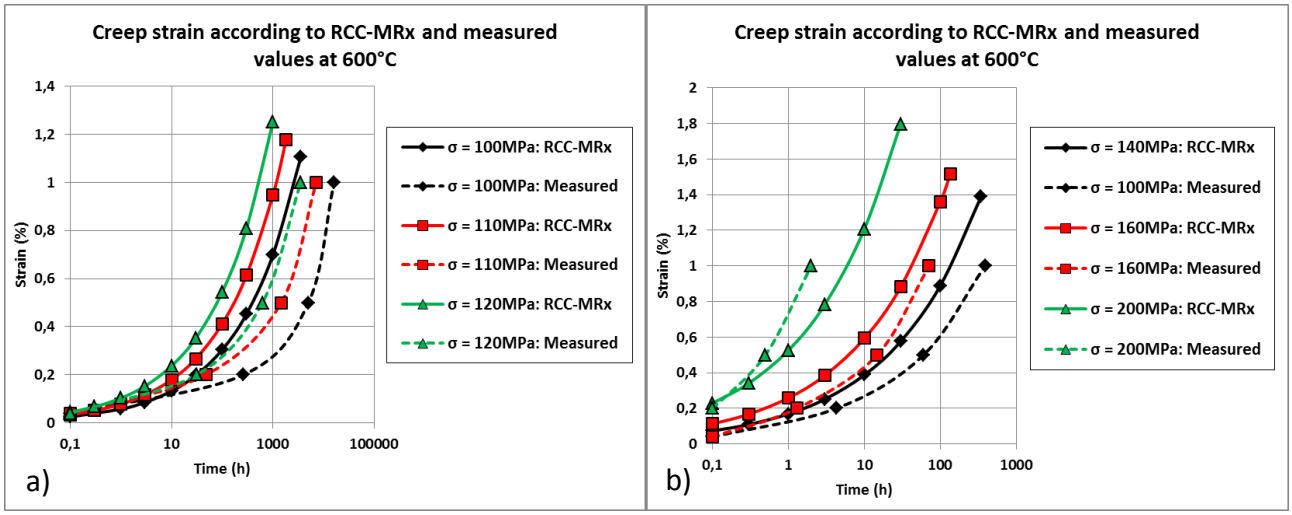

Figure 9. Creep test results for P91 steel at 600°C and creep strain according to RCC-MRx probationary phase rules for a) 100-120MPa and b) 140-200MPa.

Based on the evaluation results the RCC-MRx creep strain calculation procedure seems to overpredict the creep strain at low stress levels, where the rules actually apply for creep strain evaluation. This is understandable from the conservatism point of view, and probably the creep strain rule coefficients are optimized for low stress values. However, this cannot be confirmed since the RCC-MRx code does not provide any references or explanation for the coefficients to calculate the creep strain shown in Table 2.

For high stress levels, where the rules do not actually apply for creep strain evaluation, the rules seem to give non-conservative predictions for creep strains. However, this actually increases the conservatism for creep component in the creep-fatigue interaction diagram for high stress levels, since creep and relaxation are both manifestations of the same molecular mechanisms, and underpredicting the creep or relaxation rate increases the creep component in the interaction diagram. Figure 10 shows the creep-fatigue assessment using time fraction (TF) approach according to RCC-MRx for creep-fatigue tests performed in MATTER project and literature data [14]. The data points in green colour in the plot are evaluated by taking the stress relaxation during the hold period into account using the RCC-MRx relaxation assessment procedure based on the creep strain rules. The data points in red colour in the plot are the same data points assessed using the peak stress at the beginning of the hold period without taking the stress relaxation into account. It should be noted that the evaluation for data for both with and without stress relaxation behaviour is here performed without the safety margin of σ/0.9 for stress level from RCC-MRx, which would have significantly increased the creep component in both evaluations. However, Figure 10 indicates that the stress relaxation has strong impact on the creep component in the RCC-MRx assessment procedure based on the interaction diagram. If the stress relaxation is not taken into account the creep component can increase by two orders of magnitude.

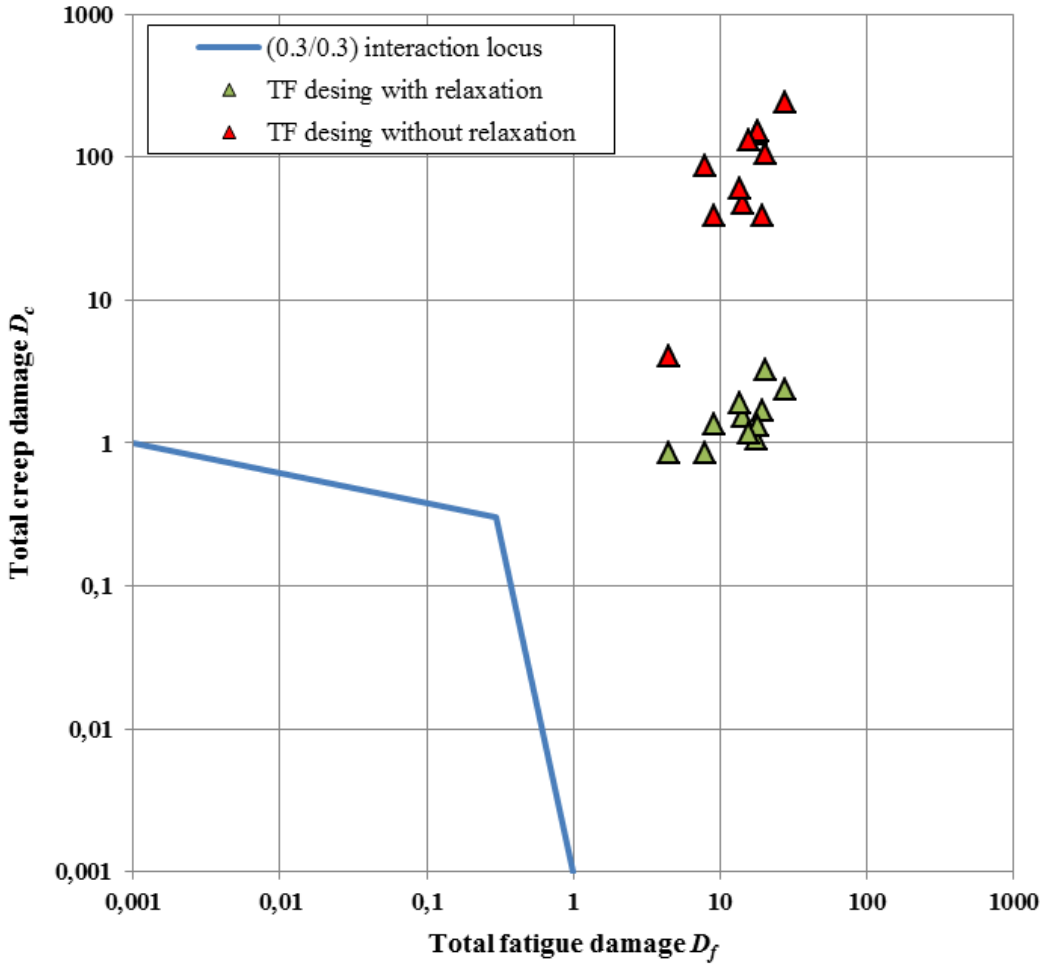

Figure 10. The creep-fatigue assessment using time fraction (TF) approach according to RCC-MRx for creep-fatigue tests performed in MATTER project and literature data [14].

3.2.1.1 Impact of softening on creep strain rate and rupture life

The RCC-MRx creep strain rules described above do not take the material characteristics, such as cyclic softening for P91 steel, directly into account. During the MATTER project, a small creep test programme was performed by JRC with pre-fatigued test specimen. The test matrix and results of the tests are presented in Table 2. The specimens were fatigued to a fatigue life fractions of LF_F =26, 52 and 78% at 550°C with a total strain range of $\Delta\varepsilon$= 0.7%. The low cycle fatiguing was interrupted at 1000, 2000, and 3000 cycles and then creep tested at 600°C with a stress of 155 MPa. The low cycle fatigue test conducted to the end of fatigue life, i.e. to 25% load drop of the steady state linear softening, gave 3860 cycles. The creep curves of the pre-fatigued and virgin material tests are given in Figure 11.

Table 4. Creep rupture time, minimum creep rate and creep life fraction for virgin and pre-fatigued (softened) P91 steel at 600°C/155 MPa. The pre-fatigue life fraction LFF before creep test and the calculated creep life ratio LFC are also given. NA=Not Applicable.

Test type	Cycling N	LF_F	σ_{pN}/σ_{p0}	t_r (h)	dε/dt min (1/h)	LF_C
Creep	0	0%	NA	665	$7.6 \cdot 10^{-5}$	100%
Fatigue→Creep	1000	26%	79%	562	$7.9 \cdot 10^{-5}$	85%
Fatigue→Creep	2000	52%	74%	293	$1.3 \cdot 10^{-4}$	44%
Fatigue→Creep	3000	78%	70%	127	$2.7 \cdot 10^{-4}$	19%
Fatigue	3860	100%	NA	NA	NA	NA

The results show that the primary creep strain rates up to around 0.5% of strain seem to be nearly unaffected by the pre-fatiguing. It seems that the pre-fatiguing is moving the location (in strain) where the minimum strain rate is achieved towards lower values the more the sample has been pre-fatigued. In Figure 12 and Figure 13 strain rates are plotted as a function of time and strain correspondingly. The results clearly indicate that prior low cycle fatigue damage (softened material) has a shortening effect on the creep life though it seems that the main effect is in secondary and tertiary creep regimes.

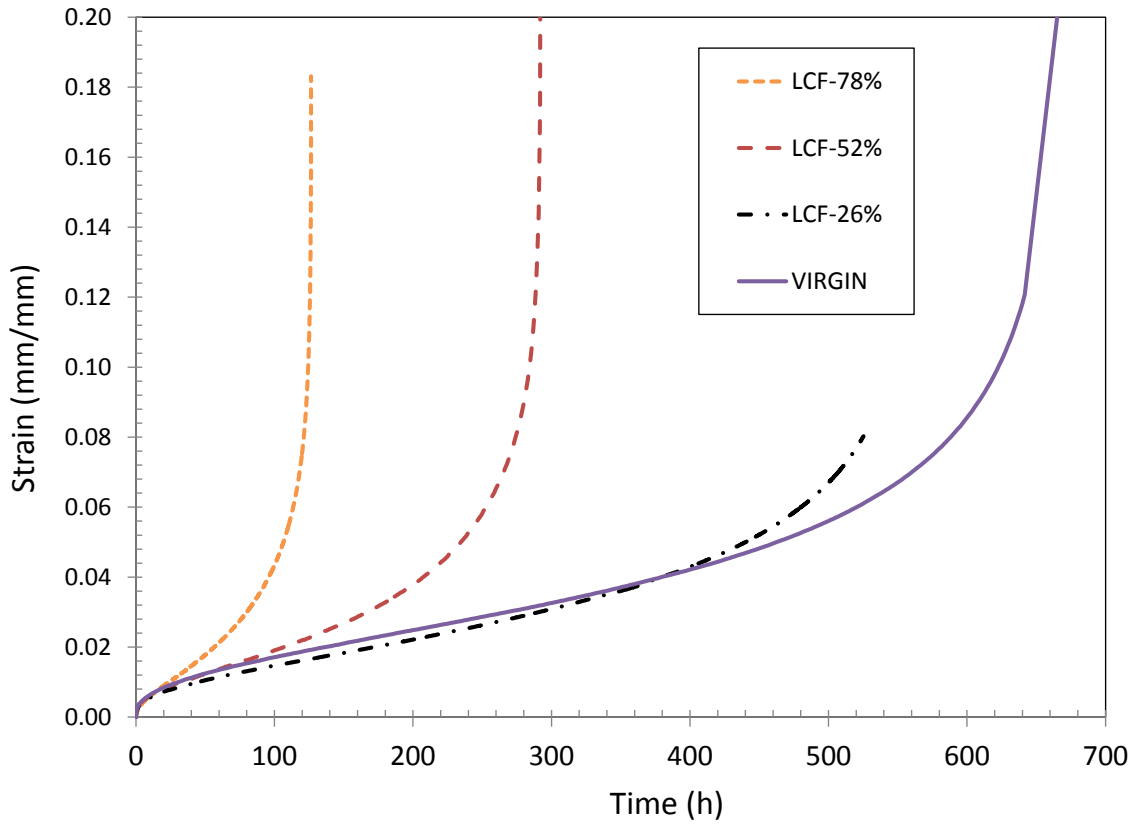

Figure 11. Creep curves for the full 155 MPa / 600°C creep test and the pre-fatigued test specimens with a LF_F = 25%, 52% and 78%.

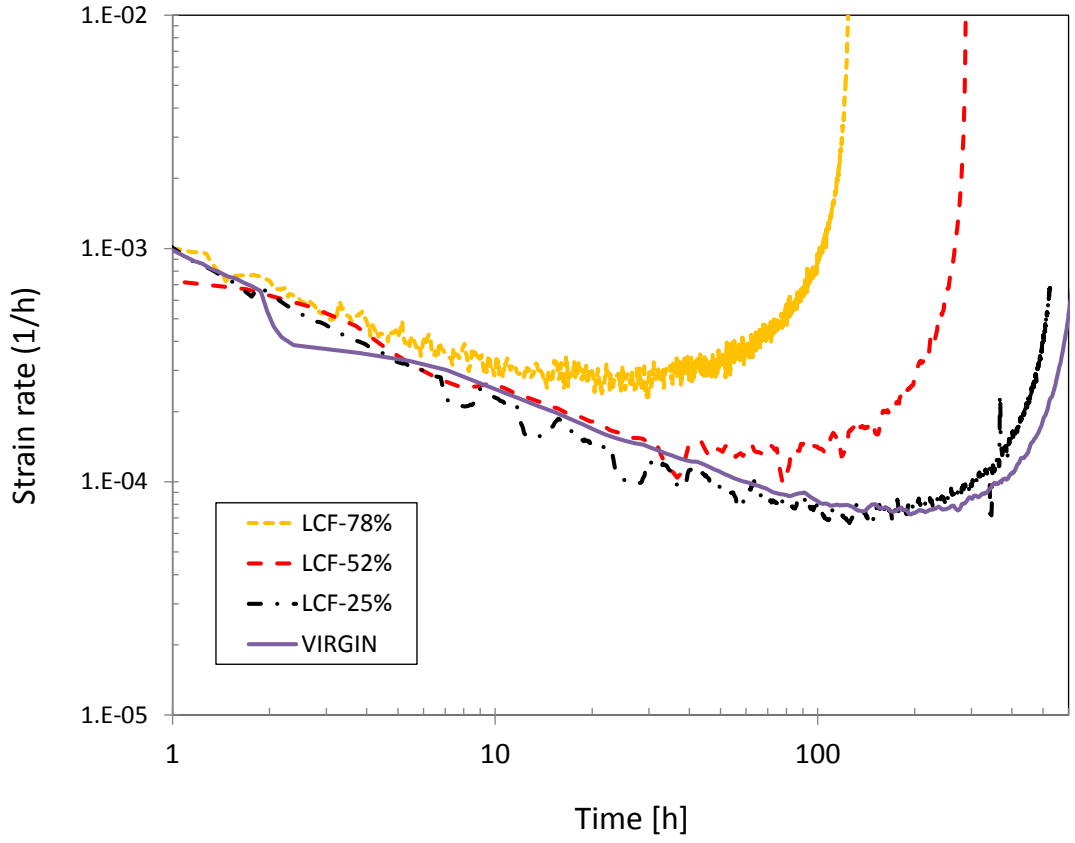

Figure 12. Creep rates as a function of time for the virgin and pre-fatigued material.

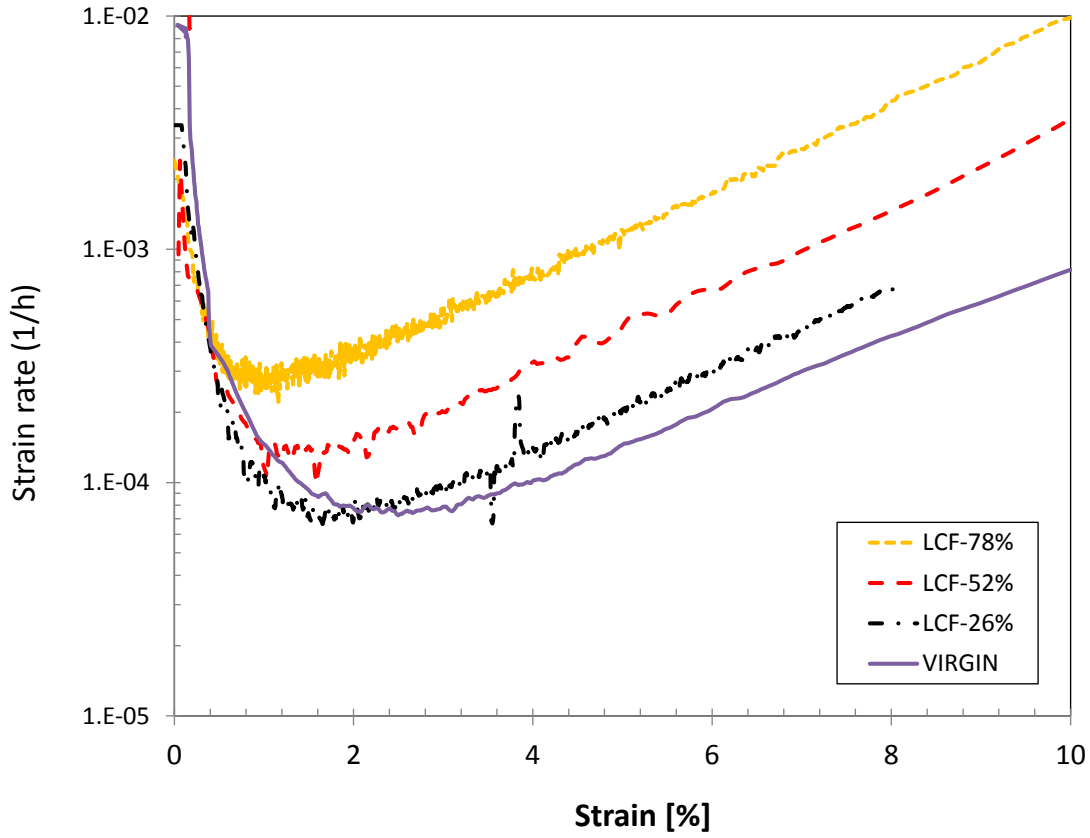

Figure 13. Creep rates as a function of strain for the virgin and pre-fatigued material. Note that the location of minimum creep rate is moving towards lover values for increased pre-fatiguing.

It can be seen that the pre-fatigue has affected the creep life and the secondary creep strain rate of the material. Note that the effect is rather small in rupture life and strain rate increase (up to a factor of 5 for LF_F=78%) in comparison to the primary creep strain rate increase evaluated from CF tests with stress controlled hold times (described later in this report). The measured effect is small also when comparing to earlier studies [17], [20] where minimum creep rates were measured after cyclic softening to $N_f/2$ could be as much as 100 times higher than those of the corresponding virgin material. For these results it is to be remembered that the stress range is very high and the high values could be caused by testing in the power-law breakdown regime.

The increase in strain rate due to softening may be problematic for designing with creep strain limitations. However, based on the above it seems that the creep strain model in RCC-MRx probationary phase rules would predict satisfactorily to about 0.5% creep strain even for the softened material. From the creep-fatigue stand point this is also not a major problem since a decreased amount of relaxation will increase the predicted creep time fraction, thus adding conservatism in the CF prediction. Also the interaction diagram is intended to take this affect into account by the non-unity locus point.

The results and reasoning above is also good news for determination of the negligible creep range for P91. If material softening is only marginally affecting the primary creep rates the negligible

creep temperature curves based on virgin material are also not affected. More test and assessments has of course to be done to verify this.

The impact of the softening on the creep properties have a clear impact for design in the case of stress controlled secondary stresses, but it might be considerably less than measured from stress controlled hold time tests.

3.2.2 Alternative creep strain models

There are several options to a more advanced approach in creep strain modelling. Some of the state-of-the-art models used for describing the whole creep curve covering the whole temperature and stress range, i.e. primary, secondary and tertiary creep stages, have a large number of material parameters. Some models have a large number of parameters like 26 fitting constants for the theta model [21] compared to the more moderate 11 for the Japanese (JAPC) model used in the ANSTO relaxation assessments in [2] and 7 for the below described LCSP model [22], [23] (both excluding rupture model parameters). Simpler models with a reasonable number of fitting constants and good prediction capability are quite rare, but do exist. In the European Creep Collaborative Committee (ECCC) project "Advanced creep" a round robin [24] was performed analysing classical model equations together with some at the time new approaches (see Table 5).

The round robin recognized 3 main approaches for model fitting:

1. Modelling individual creep curves and establishing curve model parameters
   $\Rightarrow$ determination of stress and temperature dependence of these model parameters (examples: Mod. theta, Mod. Omega, BJF and Li-Akulov)
2. Producing synthetic data from the raw data in certain coordinates ε(T,σ, t)
   $\Rightarrow$ parametric model fitting to synthetic data (examples: MHG and the modified Sandström model)
3. Producing synthetic data σ(T, ε, t) from ε(T,σ, t) raw data
   $\Rightarrow$ model fitting to synthetic data (examples: Mod. Graham-Walles and Bolton)

From these the approaches the 2 and 3 were producing the best fits for both a P22 single heat data set and a P91 multi cast strain data sets (see Table 6) The tabulated Z factor [25] describes the predictive capability of the model according Equations (11) and (12) and the smaller the number is the better.

$$RMS = \sqrt{\frac{\Sigma(\log(t_{\mathrm{mod}}) - \log(t_{meas}))^2}{n-1}} \tag{11}$$

$$Z = 10^{2.5 \cdot RMS} \tag{12}$$

With the factor 2.5 in the Z equation the true time to rupture or strain t_{pred} would lie in almost 99% of the observed times within the boundary lines defined by the scatter factor Z:

$$\log(t_{pred}) = \log(t_{\mathrm{mod}}) \pm \log(Z) \tag{13}$$

A perfect prediction by the master-equation would be represented by Z equal to unity.

Table 5. Review of the ECCC round robin strain models [24].

Model reference	Creep equation
Norton, (Norton, 1929)	$\dot{\varepsilon}_{f,\min} = d_1 \exp(-Q/RT)\sigma^n$
Modified Norton	$\dot{\varepsilon}_{f,\min} = b_1 \exp(-Q_B/RT)\sigma^n + c_1 \exp(Q_C/RT)\sigma^n$
Norton–Bailey	$\varepsilon_f = d_1\sigma^n t^p$
Bartsch	$\varepsilon_f = e_1 \exp(-Q_1/RT)\sigma \exp(-b_1\sigma)t^p$
(Bartsch, 1995)	$+ e_2 \exp(-Q_2/RT)\sigma \exp(b_2\sigma)t$
Garofalo, (Garofalo, 1965)	$\varepsilon_f = \varepsilon_t[1 - \exp(-b_1 t)] + \dot{\varepsilon}_{f,\min} t$
Modified Garofalo	$\varepsilon_f = \varepsilon_{f1}[1 - \exp(-g_1(t/t_{12})^u)$
(Granacher, *et al.*, 2001)	$+ \dot{\varepsilon}_{f,\min} t + c_{23}(t/t_{23})f]$
BJF	$\varepsilon_f = n_1[1 - \exp(-t)]^{\beta} + n_2 t$
(Jones and Bagley, 1996)	where $t = (\sigma/A_1)^n \exp(-Q/RT)$
Li–Akulov model	$\varepsilon_f = \frac{\dot{\varepsilon}_{f,\min}}{k} \ln\left(1 + \frac{\dot{\varepsilon}_i - \dot{\varepsilon}_{f,\min}}{\dot{\varepsilon}_{f,\min}}(1 - \exp(-kt))\right) + \dot{\varepsilon}_s t$
(Li, 1963; Akulov, 1964)	$+ \varepsilon_T(\exp(t/t_t) - 1)$
Theta	$\varepsilon_f = \theta_1[1 - \exp(-\theta_2 t)] + \theta_3[\exp(\theta_4 t) - 1]$
(Evans and Wilshire, 1985)	where $\log(\theta_i) = a_i + b_i T + c_i\sigma + d_i\sigma T$
Modified Theta	$\varepsilon_f = \theta_1[1 - \exp(-\theta_2 t)] + \theta_m t + \theta_3[\exp(\theta_4 t) - 1]$
	where $\theta_m = A\sigma^n \exp(-Q/RT)$
Graham–Walles	$\varepsilon_f = at^{1/3} + dt + ft^3$
(Graham and Walles 1955)	
Modified Graham–Walles	$\dot{\varepsilon}_f = e^{(Q_1/T)} 10^{A_1} \left(\frac{\sigma(1+\varepsilon)}{1+\omega}\right)^{n_1} \varepsilon^{m_1}$
	$+ e^{(Q_2/T)} 10^{A_2} \left(\frac{\sigma(1+\varepsilon)}{1+\omega}\right)^{n_2}$
	where $\dot{\omega} = e^{(-QD/T)} 10^{AD} (\sigma(1+\varepsilon))^{nD} \varepsilon^{mD}$
Rabotnov–Kachanov	$\dot{\varepsilon} = \frac{h_1\sigma^n}{(1-\omega)}\dot{\omega} = \frac{k_1\sigma^v}{(1-\omega)^{\zeta}}$
(Kachanov, 1986)	
Dyson and McClean,	$\dot{\varepsilon}_f = \dot{\varepsilon_0}(1 + D_d)\exp(-Q/RT)\sinh\left(\frac{\sigma(1-H)}{\sigma_0(1-D_p)(1-\omega)}\right)$
(Dyson and McClean, 1998)	
Baker–Cane model	$\varepsilon_f = At^m + \varepsilon_p + \phi\varepsilon_s + \varepsilon_s(\lambda - \phi)\left[I - \frac{t/t_u - \phi}{1-\phi}\right]^{\frac{1-\phi}{\lambda-\phi}}$
(Baker and O'Donnell, 2003)	where $I = \varepsilon_u/\varepsilon_s$, $\varepsilon_s = \dot{\varepsilon}_m t_u$ and $\phi = t_p/t_u$
Mech. E (CSWP, 1983)	$R_{u/t/T} = (a_1 + b_1/\varepsilon - c_1\varepsilon^2)R_{\varepsilon/t/T} + d_1 + e_1/\varepsilon + f_1/\varepsilon^2 - g_1\varepsilon^2$
Characteristic strain	$\varepsilon_f(\sigma) = \varepsilon(R_{u/t/T}/R_{\varepsilon/t/T} - 1)/(R_{u/t/T}/\sigma - 1)$
model (Bolton, 2005a)	
MHG model, (Grounes, 1969)	$t_\varepsilon = \exp(TF(\varepsilon, \sigma) + C)$ where the $F(\varepsilon,\sigma)$ function is
(Holmström and	freely selected from multilinear combinations of σ
Auerkari, 2004)	and ε with an optimised value of C
Omega, (Prager, 1995)	$\dot{\varepsilon}_f = \dot{\varepsilon}_{f,\min}/(1 - \dot{\varepsilon}_{f,\min}\Omega t)$
Modified Omega	$\varepsilon_f = \left(\frac{1}{\Omega} - \frac{1}{2C_{tr}}\right)(-\ln(t_u - t) + \ln(t_u))$
(Merckling, 2002)	$+ C_{tr}(1 - \exp(m_{tr}t))$

Table 6. Summary of Z values associated with model-fits to P91 steel data set [24], the smaller the Z value the better fit.

Model equation	Fitting approach	Z values to specified strains in %				
		0.2	0.5	1.0	2.0	5.0
Modified theta model	1	74	19	17	8	12
BJF model	1	113	104	50	32	11
Li-Akuluv model	1	143	42	18	6	4
Modified Graham-Walles model	3	7	7	6	7	5
Bolton model	3	38	7	7	6	5
MHG model	2	6	7	6	6	5
Modified omega model	1	138	19	11	8	5
Modified Sandström model	2	11	7	6	6	6

Since the round-robin [24] a new model has been developed with comparable (as good) ability to predict the same data sets as given above. The logistic creep strain prediction (LCSP) model [23], which is simple in its formulation, is based on fitting a logistic shape function to the full creep strain curves (or tabled stress to specific strain/time values) with the true time to rupture value as end point. This approach would clearly avoid the mismatch on strain curves and rupture times, which may occur if the creep strain model does not take the creep to rupture values into account.

In the ASTM round robin on Creep-Fatigue [15] it was found that from the evaluation of models mainly covered in [26] the most suitable model for P91 steel is indeed the above mentioned LCSP model. The authors did however propose some modifications to improve the prediction at very short times and at the very end of the creep curve.

The original LCSP, giving time to specified strain:

$$\log(t_\varepsilon) = \frac{\log(t_r)+C}{1+\left(\frac{\log(\varepsilon)}{x_0}\right)^p} - C, \tag{14}$$

Or in reversed form giving strain at specified time:

$$\log(\varepsilon_t) = \left(\frac{\log(t_r)+C}{\log(t_\varepsilon)+C} - 1\right)^{1/p} \cdot x_0, \tag{15}$$

Where x_0 and p are temperature and stress dependent variables and C is a material constant.

For P91 the x_0 and p variables were extracted from Equations (16) and (17) using the full creep strain curves from data by NIMS [19]. The best fit values for p_i, x_i and C parameters are shown in Table 7.

$$x_0 = x_1 + x_2 \cdot \log(\sigma) - x_3/(T+273) \tag{16}$$

$$p = p_1 + p_2 \cdot \log(\sigma) + p_3/(T+273) \tag{17}$$

Table 7. LCSP creep strain model fitting parameters for P91 steel.

Material	x_1	x_2	x_3	p_1	p_2	p_3	C
P91	-2.24	1.37	-3170	4.21	-7.27	14200	3.5

The main advantages of the model is that any creep rupture model or creep rupture data from testing can be used as input for the strain model and that the creep strain rate can be derived implicitly as a function of temperature, stress and time:

$$\dot{\varepsilon} = -\varepsilon \cdot k_1 \cdot k_2 \cdot x_0 \tag{18}$$

Where the factors k_1 and k_2 are functions of time to strain.

The LCSP model can directly be used in relaxation calculation in creep-fatigue interaction diagram predictions.

Another rupture based creep strain model with simple formulations for creep strain rate and minimum creep rate is the Bolton model [27]. This model has not been assessed in this project but could potentially be used in the same manner as the LCSP. Recommendations for selecting a suitable creep strain model are given in [28] and [29].

3.2.2.1 Impact of softening on primary creep strain rate

The MATTER CF tests with hold times in stress control (by ENEA) were analysed by applying an existing creep strain model, the logistic creep strain prediction (LCSP) for predicting the creep strains at specified hold time lengths. The LCSP was initially calibrated to give measured creep strain at end of the 2nd cycle hold time. Then the stress reduction needed to again equal the measured creep strains at the end of the hold times were solved for each reported cycle. The calculated stress correction factors for the tests with a $\Delta\varepsilon$=1% and 32 and 140 second hold times are shown in Figure 14. Note that at $N_f/2$ the stress correction factor is in the range 1.3-1.35 corresponding surprisingly well with the expected peak stress softening (see Figure 15). There is a possibility that the softening ratio could be used as a "damage" factor for estimating the loss of creep strength in the softening material. In these tests the nominal creep rate ($1/t_r$) calculated at $N_f/2$ gave increased creep rates by factors ranging from 100 to 600 in time. It is to be noted that the stress levels in question give creep rupture times in the range of minutes to hours, indicating that the high measured strain rates are likely to be an effect of being close or within the power law break down creep regime. Also, the models used were initially designed to give predictions for larger creep strains and at much longer durations.

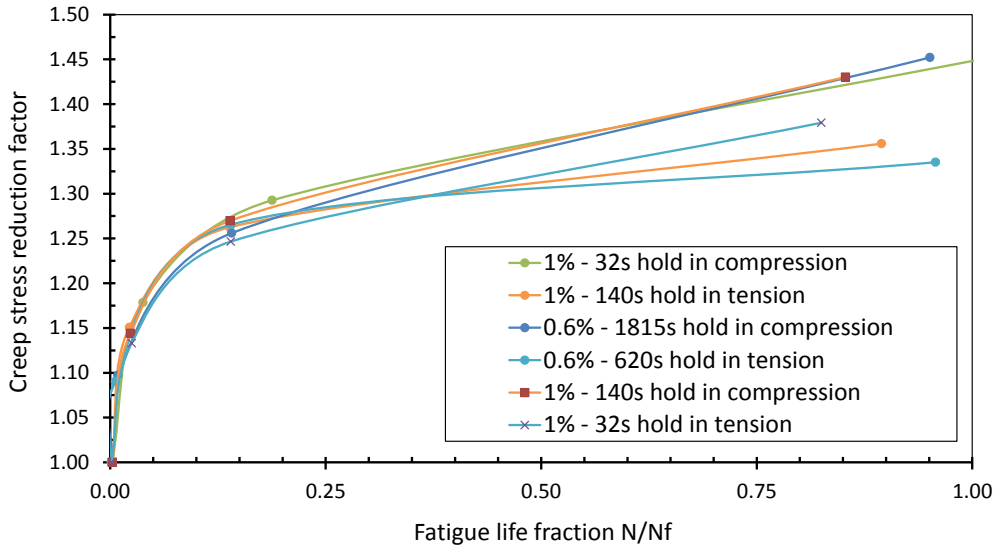

Figure 14. Calculated creep stress reduction factors for the cyclic forward (primary) creep curves at 550°C for a nominal strain range of 0.6 and 1%.

The analysis of the stress controlled hold time tests reveal that the test strain rates are incredibly high causing significant creep strain in the relatively short hold times. It is to be recommended that tests at low strain range and very long hold times should be conducted to increase the probability to cause creep cavitation damage instead of excessive creep strain.

Another way assessing the above tests is by applying the Wilshire equations [30] on the time to strain curves (see Figure 16).

The Wilshire normalized stress σ/R_m for rupture strength is defined as:

$$\frac{\sigma}{R_m} = \exp\left[-k(t_r \cdot \exp(\frac{-Q}{R \cdot T}))^u\right] \quad (19)$$

where *k* an *u* are fitting parameters, σ the test stress, R_m the ultimate tensile strength, Q the activation energy, R the gas constant and T the absolute temperature.

The time to strain curves are defined in the same way with t_ε instead of t_r with optimized values of k and u.

In this approach it is assumed that the material softening has the same impact on both peak stress and ultimate tensile strength, implying that the actual normalized stress is not changing even though the material softens. This would be seen in a test as a nearly constant creep strain at the end of the hold time even though the peak stress decreases from progressing softening. This seems to be the case for most tests after the first tens of cycles until approximately half life. Comparing the cyclic creep rates at the end of hold time against the creep rate of a virgin material the creep strain rate of a test is calculated by linear regression between the time to 0.2% and the time to 0.5% creep strain. The creep rate for virgin material at σ/R_m=0.56, where the stress is

selected from average measured stress ratios of the tests after a few tens of cycles, is 0.0003 1/h. The strain rate for softened material with an unchanged tensile strength can then be solved by dividing the normalized stress with the softening ratio. The softening ratio $R_{\sigma SR}$ can be calculated utilizing the cyclic softening curves of P91 steel, for which an example curve is shown in Figure 15, by:

$$R_{\sigma SR} = {}^{\sigma_{peakN}}/_{\sigma_{peakN_0}} \tag{20}$$

Where σ_{peakN} is the peak stress of Nth cycle and σ_{peakN_0} is the peak stress of the first cycle.

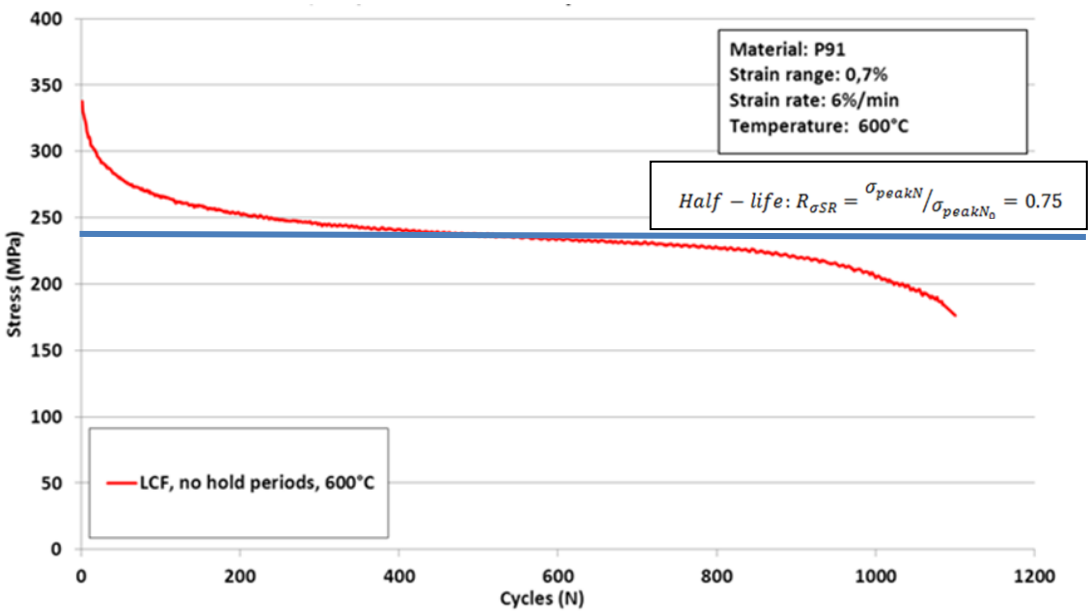

Figure 15. The peak stress as a function of number of cycles for P91 steel specimen LCF-tested at 600°C.

For a specimen that has been cycled to half-life ($N_f/2$), the softening ratio $R_{\sigma SR}$ is around 0.75. The softening ratio corrected normalized stress is then σ/R_m / $R_{\sigma SR}$ = 0.75 R_m. The calculated strain rates at these normalized stresses (σ/R_m=0.75 and σ/R_m=0.56) are 0.036 1/h and 0.0003 1/h correspondingly, which means strain rate increase of a factor of 115. This correlates also well with the calculated LCSP results and the creep rate acceleration given in [17] and [20]. It is to be noted that minimum strain rates are measured in forward creep at somewhat higher strains (1-2%) and the here calculated strain rates are linearly acquired values between 0.2 and 0.5% strain that are situated in the primary creep region.

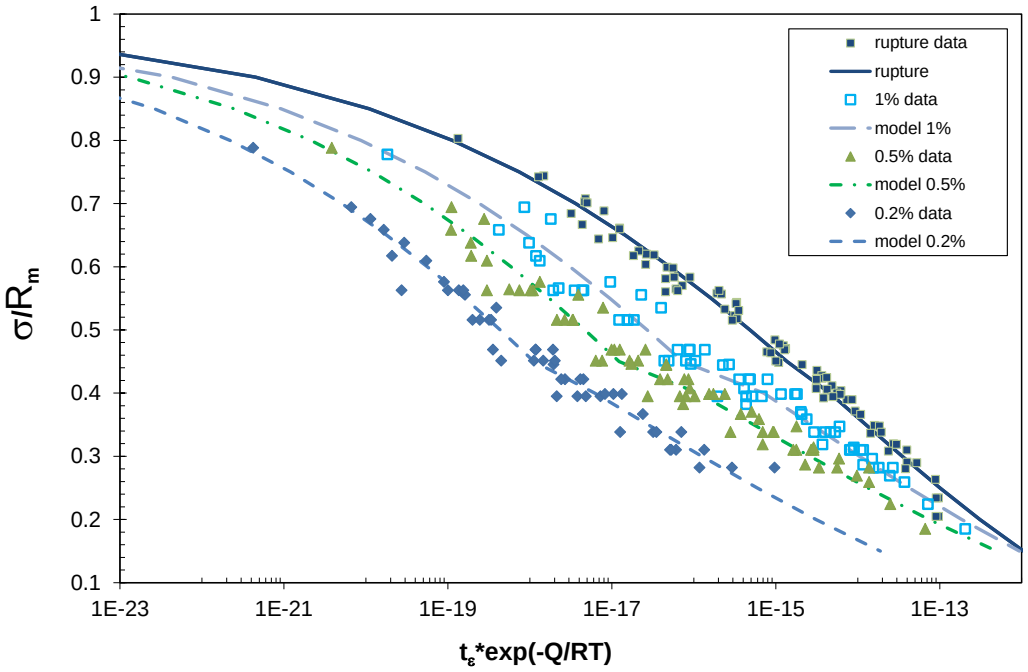

Figure 16. Wilshire creep strain models optimized on NIMS creep data [19].

For the low cycle pre-fatigued test presented earlier in this report (see Figure 11) the above method gives a minimum strain rate change of a factor of around 15 when assuming that the minimum strain rate is located at about 0.5% of creep strain and using the measured softening ratio (70%) of the test at a fatigue life fraction of 78%. The measured strain rate and rupture life reduction was only by a factor of 5, indicating that the above methodology seems to work for the stress controlled hold time tests but calibration is needed when applying it on pre-fatigued creep tests. The concept of using the softening ratio as a damage parameter is promising but clearly needs further refinement.

3.3 Creep-fatigue assessment methods

3.3.1 Creep-fatigue evaluation according to code procedures

The creep-fatigue assessment procedures and safety margins of nuclear codes have been evaluated in several studies for Gen-IV nuclear applications [2], [3], [8], [14], [31], [32], [33]. It has been shown that interaction diagram models differ considerably in the definition of the accumulated creep damage. Especially the relaxation behaviour and calculation of the creep damage fraction related to rupture time, creep ductility exhaustion or energy based methods have very strong impact on the estimated cycles to failure in creep-fatigue. The interaction diagram models are at the time the only type of models currently applied in design codes.

A creep-fatigue interaction diagram based evaluation according to RCC-MRx, ASME-NH and DDS with data obtained from various organizations such as Japan Atomic Energy Agency (JAEA), Electric Power Research Institute (EPRI), Oak Ridge National Laboratory (ORNL), Central Research Institute of Power Industry in Japan (CRIEPI), National Institute of Material Science in Japan (NIMS), and The University of Tokyo is shown in Figure 17. The data set includes CF data for P91 steel with different

thermal aging history and testing environment, for which a more detailed description is given in [14]. In this assessment, both creep and fatigue fractions resided well above the interaction diagram provided by nuclear codes, as shown in Figure 17. Similar results were obtained when CF tests performed in MATTER project were evaluated, as shown in Figure 10.

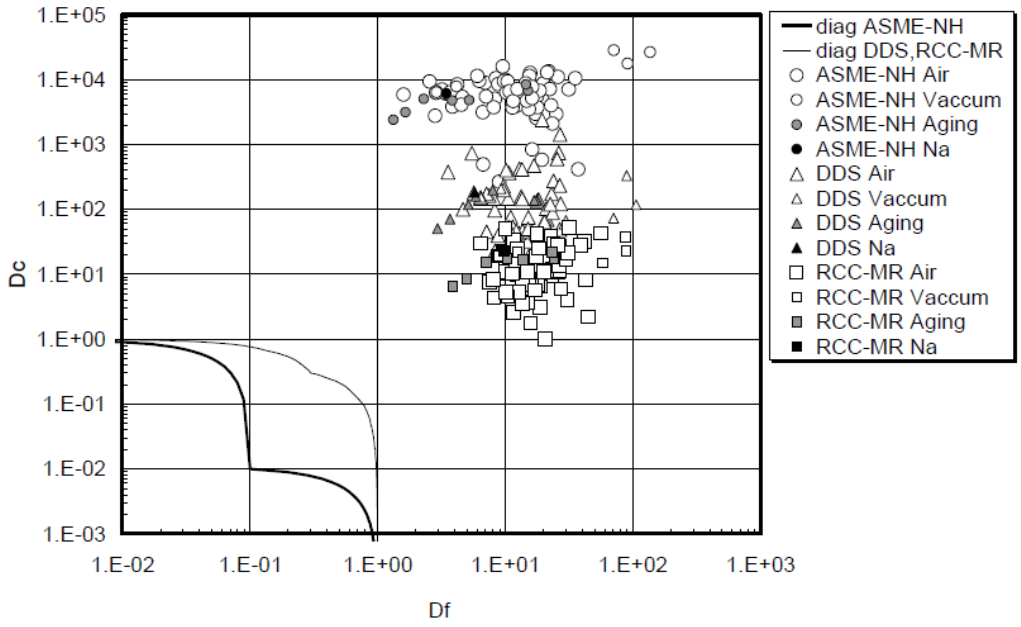

Figure 17. Creep-fatigue evaluation of experimental data by nuclear code procedures [14].

When assessing CF tests with relatively large strain ranges and short hold or creep periods, the nuclear code creep-fatigue assessment procedures, although differ considerably from each other in the definition of the accumulated creep damage, seem to provide sufficient level of conservatism for safe design. But does the sufficient level of conservatism still remain with parameters relevant to power plant conditions? Can this type of test results and assessment and modelling methods emerging from them be extrapolated to Gen-IV relevant conditions, where the stress and strain levels are lower, hold periods are significantly longer and lifetimes of components are expected to be about 60 years? Are there enough data and information on the long term microstructural evolution and its effect on the creep and cyclic properties of P91 steel?

3.3.1.1 Alternative creep-fatigue damage envelope in ASME code (CC N-812)

Creep-fatigue damage in elevated temperature design (ETD) codes, such as ASME Subsection NH and RCC-MRx, is evaluated according to the linear damage summation rule (LDSR). Creep damage and fatigue damage are separately determined based on generally elastic procedures with the introduction of various coefficients to take the inelastic behaviour into account, as shown in Figure 18. In this LDSR, the interaction effect of creep and fatigue is taken into account by limiting the allowable region in bi-linear form rather than a linear line in an envelope like that of the R5 in Figure 1.

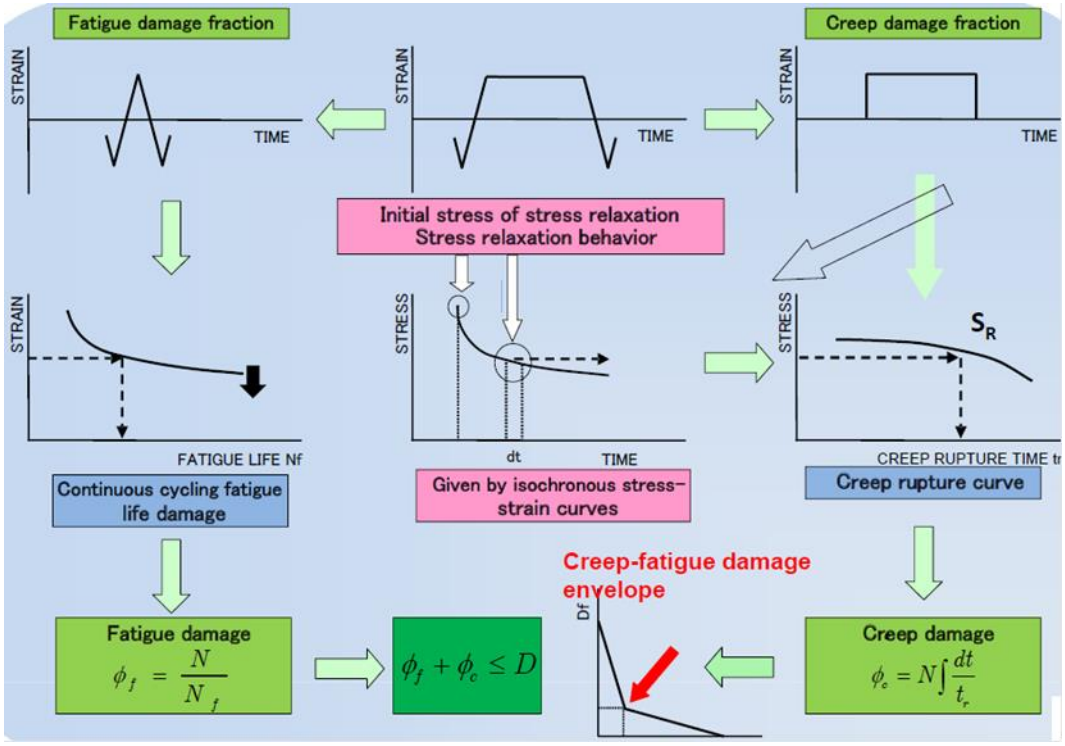

Figure 18. Procedure of creep-fatigue damage evaluation.

It should be noted that the LDSR has been developed in 1970s based on cavity growth in austenitic stainless steel at tensile hold (see Figure 19). Since creep-fatigue damage mechanism of P91 with subgrain structure is quite different from that of austenitic stainless steel and P91 is more damaging at compressive hold than at tensile hold, LDSR is known to be not appropriate for P91 in terms of damage mechanism.

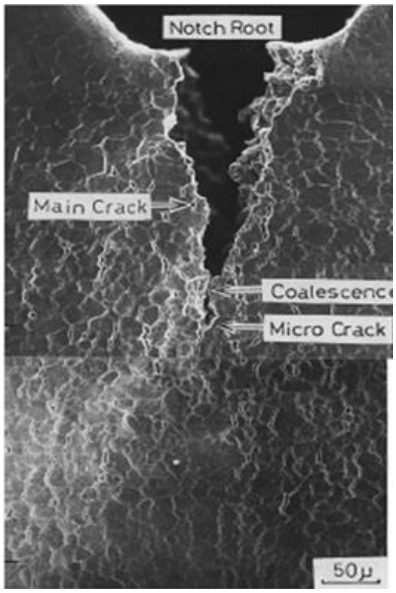

Figure 19. Creep-fatigue crack growth in austenitic stainless steel 304SS at 650°C.

The creep-fatigue damage envelope of P91 in ASME Subsection NH is known overly conservative with the intersection point of (0.1,0.01) in the envelope (see Figure 1 and Figure 20), which means

that the intersection point of 0.01 in creep damage is 1/30 compared to the value of RCC-MRx. The evaluation results shown in Figure 17 support the statement that ASME Subsection NH is overly conservative regarding to the creep component, because the data points evaluated according to ASME Subsection NH exhibit significantly larger (>1 order of magnitude) creep fractions than those evaluated according to RCC-MRx and DDS.

The subgroup committee of ASME ETD published a code case N-812 (on 1st Jan 2013) to loosen overconservatism for P91, which allows to use the creep-fatigue damage envelope with intersection point of (0.3,0.3) as shown in Figure 20. Two conditions, however, should be applied in order to use this code case:

1. The elastic analysis procedure of ASME-NH should be followed.

2. The isochronous curves in ASME-NH should be used when evaluating the creep damage.

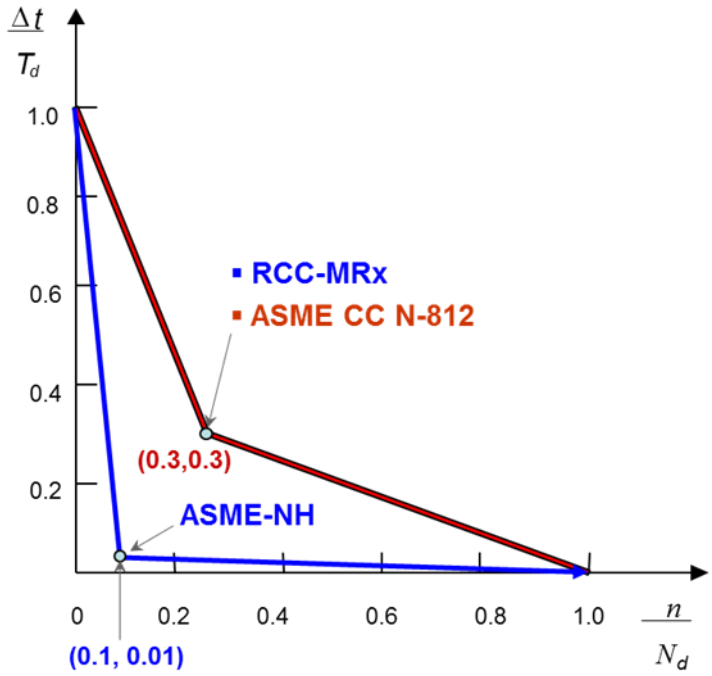

Figure 20. The creep-fatigue damage envelope in elevated temperature design codes (RCC-MRx and ASME-NH) including ASME code case N-812.

3.3.2 Simplified creep-fatigue assessment procedures

Earlier in this report it was mentioned that there is a possibility that the bulk of available data for P91 is not affected by real long term creep damage (cavitation). The use of creep amplified strain range and the LCF fatigue curves is thus not really an option since it is rather clear that it will surely not take the long term creep cavitation damage into account. The method can of course be used as reference by taking the elastic-plastic strains into account and calculate for the corresponding stresses. The creep strains would then be assessable from the creep strain models of the code in the same manner as when determining the creep life fraction for the creep-fatigue interaction diagram. Another option for simplified CF calculations in the code is to use the CF

models either based on the defined LCF curve or CF and creep rupture properties instead of the interaction diagram approach.

It has been shown in MATTER that good and robust predictions of the CF number of cycles to failure for P91 can be accomplished by these simplified methods, at least for the strain, temperature and hold time range covered by the available data. These models are not influenced by the material softening (or hardening) and have much fewer fitting parameters than any of the currently used interaction diagram methodologies. If considering the simplicity of use and the clear advantage in total amount of fitting constants needed, it is clear that the simplified methods have an advantage compared to the current code assessment procedures.

The below described simplified models are able to predict CF life with a minimum amount of variables. The approaches use LCF cycles to failure, strain range (elastic + plastic), hold time and temperature as input variables.

One of the simplified models applied in the MATTER to predict the creep-fatigue cyclic life is the Manson-Halford model (MH-CF) [13], [34]:

$$N_{CF}(t_h) = \frac{N_{f0}}{1 + \frac{k}{\frac{A}{t_h} \cdot \left(N_{f0}\right)^{\frac{m+b}{m}}}} \tag{21}$$

The model parameters *A* and *m* are derived from the creep rupture model of the material. The parameter *m* is the slope of dlog(σ)/dlog(t_r) of the creep model and *A* the rupture time at a specified reference stress. The reference stress used for P91 was the 75% ultimate tensile strength (R_m) at the specified temperature. The material constant *k* is found by fitting to available creep-fatigue data. The parameter *b* is retrieved from the Δε-N_{f0} curve by extracting the elastic exponent of the Manson-Coffin equation. The material parameter *k* is expected to be dependent on the type of control. The parameters for P91 at 550°C and 600°C optimized on the JAEA data are given in [14]. Note that t_h is to be given in hours and model is predicting strain controlled CF lives only.

It should be noted that the MH-CF model also needs the LCF cycles to failure as input. The parameters for the Manson-Halford model are given Table 8. The LCF model parameters were given earlier in this report in Table 1.

Table 8. Parameters for the MH-CF model at 550°C, log(A)= -0.0236·T + 13.961 for interpolation use in the range of 550-600°C only.

Temperature (°C)	A(T)	m	b	k
550	10	-0.0783	0.12	0.07904
600	0.6			

The Φ-model [6], [35] is based on the assumption that there exists a reference stress σ_{ref} multilinearly definable in strain range $\Delta\varepsilon$, temperature T and hold time t_h that predicts a creep rupture time equal to the combined hold times in a CF test. The model is using the Wilshire equation [30] for creep as base.

The reference normalized stress Φ_{CF} (σ_{ref}/R_m) for Φ-model is defined as:

$$\Phi_{CF}(\Delta\varepsilon, t_h, T) = A_1 + \frac{A_2}{\Delta\varepsilon} + A_3 \cdot \log(t_h) + A_4 \cdot T \tag{22}$$

Using Equation (19) and rewriting the sum of hold times causing cyclic failure becomes:

$$\sum t_h = -\left(\frac{\Phi_{CF}(\Delta\varepsilon, t_h, T)}{k}\right)^{1/u} \cdot \exp\left(\frac{Q_c^*}{RT}\right) \tag{23}$$

And the number of cycles is simply:

$$N_f = \frac{\sum t_h}{t_h} \tag{24}$$

The parameters needed for using the Φ-model for predicting CF cycles to failure are given in Table 10 (creep rupture parameters for the Wilshire equation in Table 9).

Table 9. Wilshire creep rupture model parameters for P91 steel (NIMS data [19]). Note that time ($t_{r/\varepsilon}$) is in hours, and the total strain range in %. Note also that there is a change in parameters at the stress ratio of 0.45. The activation energy Q is 300 000 J/mol in all cases.

Model type	$\sigma/R_m > 0.45$		$\sigma/R_m \leq 0.45$	
	k	u	k	u
rupture	82.769102	0.135627	75.618032	0.133624

Table 10. Parameters for the Φ-model. The parameters are optimized on JAEA data [14]. The temperature range is 450-650°C.

A1	A2	A3	A4
1.98016	-0.06706	-0.07629	-0.00162

The simplified models are successfully predicting the JRC CF test data for temperatures 550 and 600°C as shown in the predicted versus measured cycles to failure plot in Figure 21. It can be seen that even the LCF model (based on JAEA data) is describing the data points well though there is an increasing error for the longer tests. The simplified models both show conservative predictions with the Φ-model closer to the measured values.

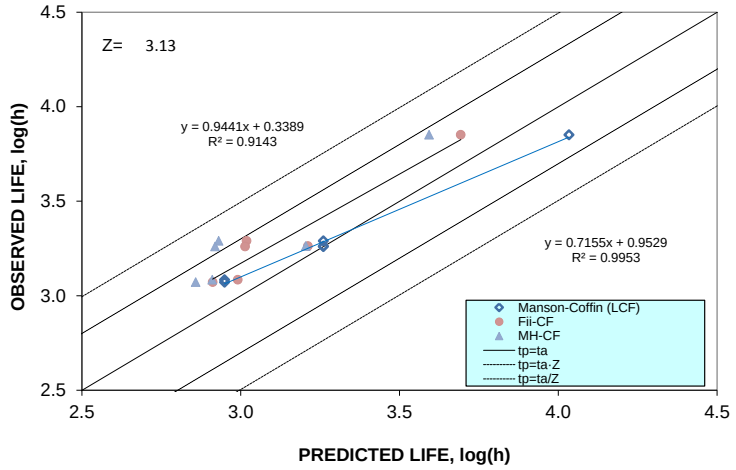

Figure 21. Predicted versus measured cycles to failure for CF tests with 0.1-0.34 h hold time using the Manson-Coffin LCF model and the Φ-model and MH-CF creep-fatigue model at 550 and 600°C.

The strain amplification methodology can be implemented also in Φ-model. A predicted versus measured plot for a MATTER creep-fatigue data set (strain corrected according to Chapter 3.1.1) produced by ENEA using Φ-model is presented in Figure 22.

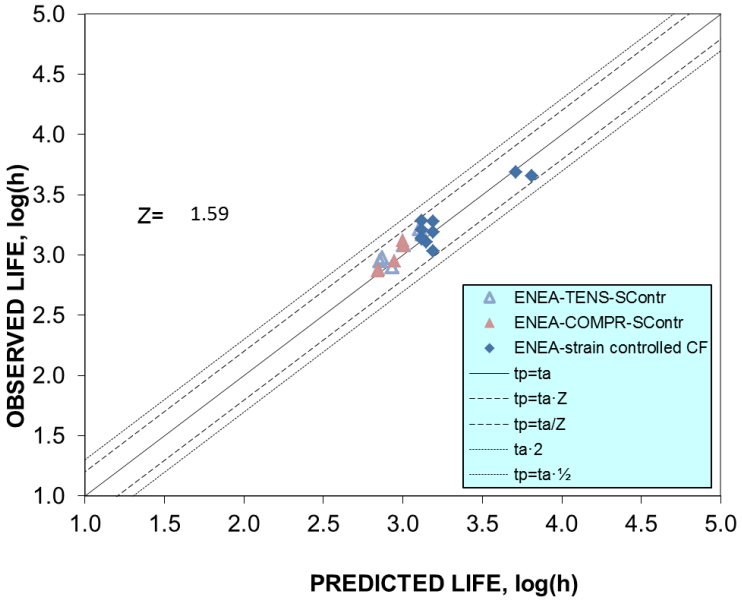

Figure 22. ENEA predicted vs. measured creep-fatigue life when correcting total strain and using Φ-model for impact of hold time. The data set includes strain and stress controlled hold times.

As a test of extrapolating outside the range of data the simplified Φ-model is tested against the average cycles to failure data at higher temperature (625°C) from the EPRI round-robin [15] for strain ranges 1 and 1.5%. The measured and predicted CF cycles to failure with hold times up to 30 min are shown in Figure 23. It can be seen that the Φ-model predicts only slightly conservative cycles to failure well within the scatter range of the round-robin indicating that the model extrapolation towards higher temperatures give robust predictions. The Manson-Halford model is predicting too conservative values and it is clear that extrapolating the A(T) parameter log-linearly towards higher temperatures does not give sensible CF predictions.

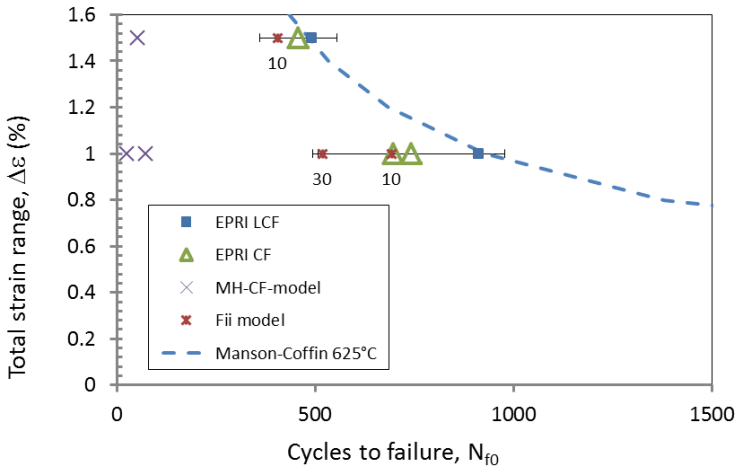

Figure 23. Simplified model predictions outside the temperature range they were fitted to. The Φ-model predicts slightly conservatively but within EPRI round robin [15] interlaboratory scatter. The hold time in minutes is given below the predicted CF data point.

4 Discussion

Looking at the available data and the present assessment results it seems that in almost all cases the laboratory creep-fatigue data have too short hold times and/or too high strain levels to give a good base for extrapolation to service conditions where creep is more dominating. The analysis of the strain controlled tests with hold times in strain or stress control verifies this by generally falling on or within the scatter band of the LCF results after adding the creep strain accumulated during hold times to the total strain range (see Chapter 3.1.1). It seems that the induced "creep damage" for the data is mainly strain amplification and is not really affected by creep damage (cavitation) in the grain boundaries that would cause intergranular fracture and reduced material ductility. The extrapolation to "long term" type of creep damage is thus questionable with the present available data.

Recent studies [17], [20] and test results presented in Chapter 3.2.1.1 indicate that the creep behavior of P91 steel is severely deteriorated after creep-fatigue cyclic loading. The minimum creep rate measured at $N_f/2$ can be up to several hundred times faster than that measured at the first cycle (when the material is in the as-received condition). These results show that when high cumulative plastic (and creep amplified) strains (several hundred percent) are applied to these materials, their creep behavior changes significantly. But as stated, the large creep rates were

measured in CF tests with hold times in stress control for stresses clearly exceeding yield (0.7 to 0.8 R_m). The applied stresses were therefore high and likely to be close or within the power law breakdown regime for the softened material. The corresponding stress level for the virgin material is in the range 0.5 R_m for the above mentioned tests.

The results from pre-fatigued (softened) material (see Chapter 3.2.1.1) should fall into the same ball park of accelerated creep rates if material softening alone is the cause of the creep rate increase. The softening ratio for the pre-fatigued tests with LF_F of 52% and 78% are about at the same level as for the CF tests (~70% of original strength). The grain structure after a pure fatigue tests and a CF test is expected and shown in [17] to be different, indicating that creep affects the microstructural development during testing. In terms of interaction diagram assessment the pre-fatigued creep tests have no prior creep damage whereas the CF tests with hold in stress control have already consumed a substantial amount of the expected creep life. As a consequence the minimum strain rate measured at $N_{f/2}$ would then intuitively correspond more to a strain rate in later life (tertiary creep). The pre-fatigued test specimens exhibited creep rates with a maximum creep rate factor of 5 for the LF_F=78% test. The actual (softened material) tensile strength values for pre-fatigued and CF tested specimen should be measured to give better understanding of the proximity of the creep test to power law break down stress region. The allowable stress for design is located at 0.37 R_m seemingly far away from where local stress concentrations in regions with softened material could reach or close in on power law breakdown levels.

To improve the understanding of creep properties of the P91 steel under cyclic loadings new data should also be generated with much longer hold times and preferably at low to very low strain ranges with creep amplification, preferably as forward creep (stress control). It is though clear that there are limitations in testing time that are difficult to overcome. Furthermore, there are also other factors that can affect the creep-fatigue life of P91 steel. Creep damage, tensile mean stress, oxidation, aging (microstructural evolution) and loading sequence effects (creep rupture strength after cyclic softening) are among these factors. The effects of oxidation, aging, and cyclic softening, which are not equally problematic in the case of austenitic steels, should be carefully addressed in the case of ferritic steels such as P91.

As far as the current design codes are concerned, it is not very practical to take every factor that can affect creep-fatigue life explicitly into account in the code procedure. Therefore, material tests should be performed systematically to identify relative importance of those factors. Large sets of very long term tests will not be necessarily needed, if tests can identify the limits where the effect of each factor saturates. Following this procedure the code assessment methods may be simplified and made more accurate.

The simplified models optimized for P91 seem to be promising and they predict cycles to failure in a robust way. Additional data in the long term hold time regime would of course improve the reliability of the models and increase the credibility of extended extrapolations. The equation(s) for simplified CF predictions is easily modified to incorporate sufficient safety factors. The method(s) could then replace the current complicated interaction diagram approach (see Chapter 3.3.2). The new methodology would totally avoid the question of the multitude of variations for "creep damage" calculated for a cycle that is assumed to be representative for the whole test. Also the impact of softening/hardening and the somewhat arbitrary defined interaction locus in the

interaction diagram would be avoided. As earlier emphasized, the main objective in selecting a model for implementation in design rules is that it should be concise and simple and that reasonable safety margins must be included. Verification calculations should of course be performed and verified against in real service (damage) cases and mock-up tests with challenging geometries.

5 Recommendations

During MATTER project, a number of methods, including interaction diagram based methods and simplified methods, have been compared for the predicting the creep-fatigue life of P91 steel using literature data and creep-fatigue data produced in the MATTER project. This section summarizes recommendations for the improvement of code procedures based on the investigations described in previous sections. By applying the recommendation 1 the creep behavior and creep component in the interaction diagram based method may be more accurately described. Recommendation 2 provides an alternative to the interaction diagram based creep-fatigue evaluation. Recommendation 3 is considered necessary for all evaluation and modelling methods.

1. Tests performed in MATTER project and recent studies indicate that the creep behavior of P91 steel is deteriorated after cyclic loadings. However, the assessment methods in codes do not take this effect properly into account. For example, in the RCC-MRx probationary phase rules the creep strain equations for primary and secondary creep region are provided for defined stress-time-temperature range along with fitting constants, but the cyclic history is not taken into account in that procedure. A way to improve the creep strain assessment in codes would be to implement a creep strain model, such as LCSP model, which limits the time to strain to a maximum value of a specified time to rupture. This approach would make corrections for softening/hardening or "creep damage" history simpler, for instance by introducing correction factors. The application of damage history of course further complicates the use of any model with the creep-fatigue interaction diagram. The main implication of the softening is not for creep-fatigue interaction in the RCC-MRx code, but rather for pure creep design. In the case of creep-fatigue an underestimation of creep rate will cause higher creep damage factors due to higher stresses to be used for creep rupture determination. Applied in the interaction diagram the result is more conservative limits for the allowable number of cycles.

2. The interaction diagram models are at the time the only type of models currently applied in design codes. The simplified models optimized for P91 seem to be very promising and they robustly predict cycles to failure with as good or superior performance. The equations of the simplified methods are also easy to implement for strain range, temperature and hold time dependent allowable cycle predictions (see Chapter 3.3.2). The new methodology would totally avoid the question of the multitude of variations for "creep damage" calculated for a cycle that is assumed to be representative for the whole test. Also the impact of softening/hardening and the somewhat arbitrarily defined interaction locus in the interaction diagram would be avoided.

3. For creep-fatigue assessment using interaction diagram based models or the recommended new simplified methods, the majority of currently available data for modelling and validation is situated in the regime of relatively large strain ranges and short hold periods, where the induced "creep damage" for the data is mainly strain and is not really affected by creep damage (cavitation) in the grain boundaries. The extrapolation to "long term" type of creep damage is thus somewhat questionable with the present available data. To properly validate either the interaction diagram based methods or the simplified methods, test data with long hold periods (in stress and strain control) is required. The tensile properties of softened material from both LCF and CF tests at different locations in the softening curve also need to be thoroughly determined to further investigate the high creep strain rates measured in CF tests with stress controlled hold times. The long to very long hold time tests may also improve the understanding of the long term microstructural evolution in cyclic service.

6 Acknowledgement

The authors wish to acknowledge the work effort of all the people involved in the material testing (WP 7.1) and data transfer to the MATTER data base (WP 4.1).

7 References

[1] RCC-MRx Code, "Design and Construction Rules for Mechanical Components of Nuclear installations," AFCEN, Paris, 2012.

[2] R. Pohja, S. Holmström, K. Nilsson, W. Payten, H.-Y. Lee and J. Aktaa, "Creep-fatigue interaction rules for P91," MATTER – Deliverable D4.5, EURATOM FP7 Grant Agreement no. 269706, 2014.

[3] S. Holmström, R. Pohja and W. Payten, "Creep-fatigue interaction models for grade 91 steel," *Materials Performance and Characterization,* vol. 3, no. 2, p. 26, 2014.

[4] ASME boiler and pressure vessel code, Section III Div. 1 Sub-Section NH, New York USA: ASME, 2007.

[5] ASME Boiler and Pressure Vessel Code, Section VIII, Division 2, Rules for Construction of Pressure Vessels – Alternative Rules, New York: The American Society of Mechanical Engineers, 2008.

[6] S. Holmström and P. Auerkari, "A robust model for creep-fatigue life assessment," *Materials Science and Engineering A,* vol. 559, no. 1, pp. 333-335, 2013.

[7] R. Pohja, A. Nurmela, P. Moilanen and S. Holmström, "Creep-fatigue properties of grade 91 steel," in *Proceedings of the 7th International Conference On Advances In Materials Technology For Fossil Power Plants*, Waikoloa, Hawaii, USA, 2014.

[8] R. Pohja and S. Holmström, "A comparison of creep-fatique assessment and modelling methods," in *Proceedings of the 22nd International Conference on Nuclear Engineering, ICONE 22*, Praque, Czech Republic, 2014.

[9] D. Bernardi, J. Aktaa, M. Blat-Yrieix, M. Bruchhausen, C. Cristalli, F. Dolci, S. Holmström, H. Lee, P. Matheron, K.-F. Nilsson, R. Pohja, W. Vincent and K. Zhang, "Synthesis of the experimental work for the design rules improvement," MATTER – Deliverable D7.1, EURATOM FP7 Grant Agreement no. 269706, 2014.

[10] R5, Assessment procedure for the high temperature response of structures, Gloucester, UK: British Energy, 2003.

[11] "Criteria of the ASME Boiler and Pressure Vessel Code for design by analysis in sections III and VIII division 2. Pressure Vessels and Piping: Design and Analysis, A Decade of Progress," ASME, 1972.

[12] B. Langer, "Design of of Pressure Vessels for Low-Cycle Fatigue," *J. Basic Eng.,* vol. 84, pp. 389-402, 1962.

[13] S. Manson, "A simple procedure for estimating high-temperature low cycle fatigue," *Experimenthal Mechanics,* vol. 8, no. 8, pp. 349-355, 1968.

[14] T. Asayama, Y. Tachibana, "Collect Available Creep-Fatigue Data and Study Existing Creep-Fatigue Evaluation Procedures for Grade 91 and Hastelloy XR, DOE/ASME Generation IV Materials Project, A report on Task 5 submitted to ASME ST-LLC, Revision 3 Final Report," JAEA, 2007.

[15] V. Kalyanasundaram, A. Saxena, S. Narasimhachary and B. Dogan, "Round-Robin on Creep-Fatigue and Creep Behavior of P91 Steel," *Journal of ASTM International,* vol. 8, no. 4, 2011.

[16] B. Fournier et al., "Creep–fatigue–oxidation interactions in a 9Cr–1Mo martensitic steel. Part I: Effect of tensile holding period on fatigue lifetime," *International Journal of Fatigue,* p. 649–662, 2008.

[17] B. Fournier et al., "Comparison of variuos 9-12Cr steels under fatigue and creep-fatigue loadings at high temperature," *Materials Science and Engineering A,* vol. 528, pp. 6034-6945, 2011.

[18] RCC-MRx Code, "Design and Construction Rules for Mechanical Components of FBR Nuclear Islands and High Temperatrure Applications, Appendix A16," AFCEN, Paris, 2010.

[19] "NIMS creep data sheet. Atlas of creep deformation property No. D-1. Creep deformation properties of 9Cr-1Mo-V-Nb steel tubes for boiler and heat exchanger," NIMS, 2007.

[20] B. Fournier et al., "Creep-Fatigue Interactions in a 9 Pct Cr-1 Pct Mo Martensitic Steel: Part I. Mechanical Test Results," *METALLURGICAL AND MATERIALS TRANSACTIONS A,* vol. 40A, pp. 321-329, 2009.

[21] J. Granacher, H. Möhlig, M. Schwienheer and C. Berger, "Creep equations for high temperature materials," in *Proceedings of the 7th Int. Conf. on Creep and Fatigue at Elevated Temperatures*, Tokyo, 2001.

[22] S. Holmström, Engineering tools for robust creep modelling, vol. A Doctoral Dissertation, Espoo: VTT Publications 728, 2010, p. 147.

[23] S. Holmström and P. Auerkari, "Robust prediction of full creep curves from minimal data and time to rupture model," *Energy Materials, Materials Science & Engineering for Energy Systems,* vol. 1, pp. 249-255, 2006.

[24] ECCC, Creep & Fracture in High Temperature Components - Design & Life Assessment Issues, A. Shibli, S. Holdsworth and G. Merckling, Eds., DEStech Publications Inc., 2005, p. 1115.

[25] S. Holdsworth et al., "Creep data validation and assessment procedures," ECCC publications, 2005.

[26] F. Abe, T.-U. Kern and R. Viswanathan, Creep-resistant Steels, Cambridge, UK: Woodhead publishing ltd., 2008, p. 700.

[27] J. Bolton, "A 'characteristic-strain' model for creep," in *Proceedings ECCC conference on creep and fracture in high temperature components*, London, 2005.

[28] S. Holmström et al., "Engineering approach to creep strain modeling for a multicast 9Cr steel," in *Proceedings of ASME PVP, PVP2006-ICPVT-11-94026*, 2006.

[29] S. Holdsworth et al., "Factors infuencing creep model equation selection," *International Journal of Pressure Vessels and Piping,* vol. 85, no. 1-2, pp. 80-88, 2008.

[30] B. Wilshire, P. Scharming and R. Hurst, "A new approach to creep data assessment," *Material Science and Engineering A,* Vols. 510-511, pp. 3-6, 2009.

[31] T. Asayama, "Update and Improve Subsection NH Alternative Simplified Creep-Fatigue Design Methods, DOE/ASME NGNP/Generation IV Materials Project, Final report on Task 10 submitted to ASME ST-LLC," JAEA, 2009.

[32] "Improvement of ASME Section III-NH for Grade 91 Negligible Creep and Creep-Fatigue," ASME Standards Technology LLC, 2008.

[33] P. Auerkari et al., "High temperature component analysis overview of assessment & design procedures," ECCC, 2005.

[34] S. Manson and G. Halford, "A method of estimating high temperature low cycle fatigue behaviour of materials," NASA Technical Memorandum - NASA TM X -52270, 1967.

[35] R. Pohja et al., "A study of creep-fatigue interaction in the nickel-base superalloy 263," in *10th Liege Conference on Materials for Advanced Power Engineering*, 2014.

European Commission
EUR 27781 EN – Joint Research Centre – Institute for Energy and Transport

Title: **Recommendation for Creep and Creep-fatigue assessment for P91 Components**

Author(s): Rami Pohja, Stefan Holmström, Hyeong-Yeon Lee

Luxembourg: Publications Office of the European Union

2016 – 43 pp. – 21.0 x 29.7 cm

EUR – Scientific and Technical Research series – ISSN 1831-9424 (online)

ISBN 978-92-79-57139-8 (PDF)

doi: 10.2790/49517

LD-NA-27781-EN-N

JRC Mission

As the Commission's in-house science service, the Joint Research Centre's mission is to provide EU policies with independent, evidence-based scientific and technical support throughout the whole policy cycle.

Working in close cooperation with policy Directorates-General, the JRC addresses key societal challenges while stimulating innovation through developing new methods, tools and standards, and sharing its know-how with the Member States, the scientific community and international partners.

Serving society
Stimulating innovation
Supporting legislation

doi: 10.2790/49517

ISBN 978-92-79-57139-8

Publications Office